Supplements

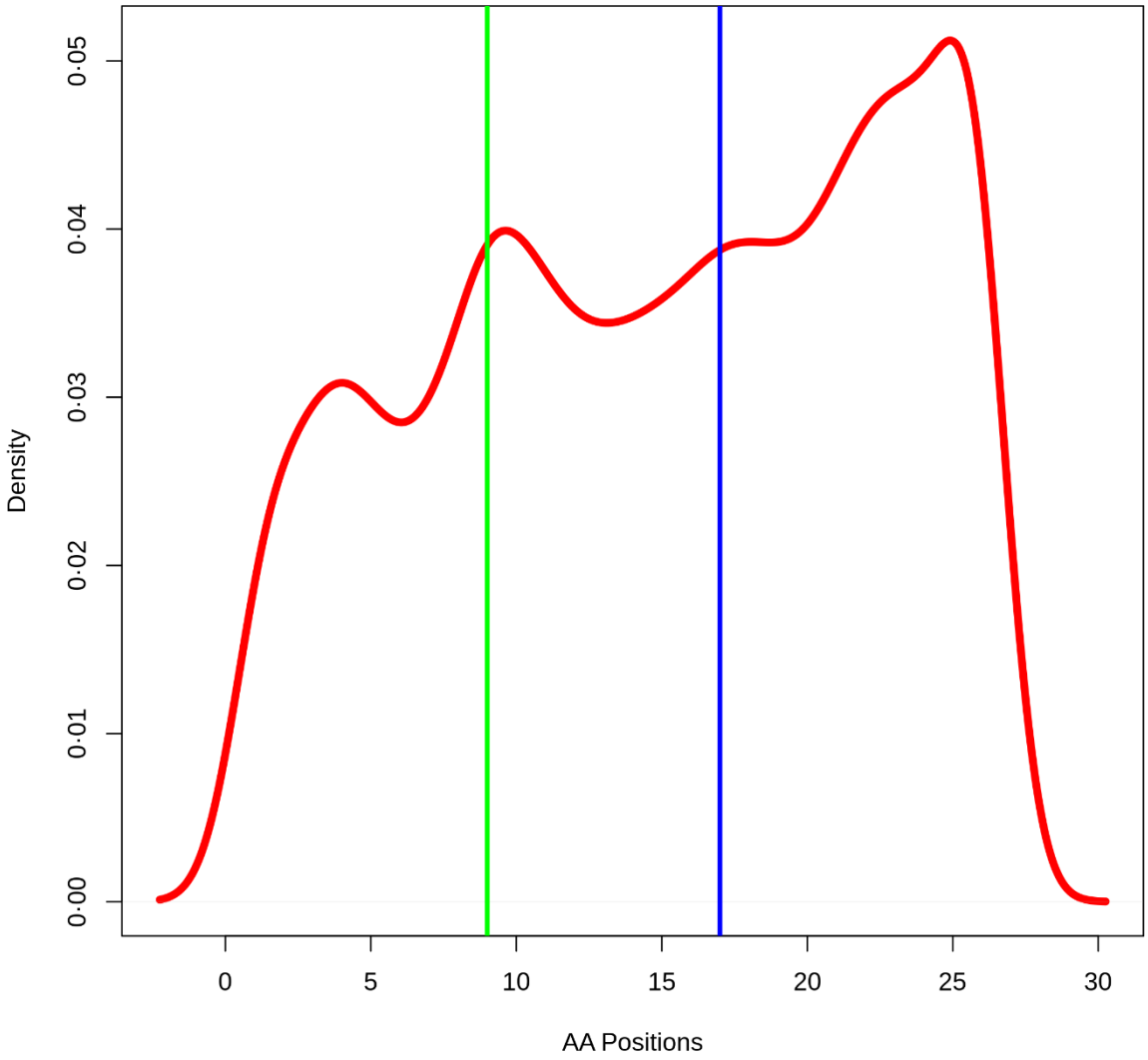

Supplementary Figure 1A: Distribution of proteasomal cleavage sites within the epitope including the flanking regions.
The figure illustrates a density plot of additional cleavage sites within our analyzed cohort of immune-checkpoint treated NSCLC patients. A major peak can be observed in the C-terminal flank spanning the positions around aa position 22 to 25. Within the actual epitope sequence (aa9 – aa17), only a minor amount of possibly additional cutting sites appears. The C-terminal flank seems not to be affected that much.

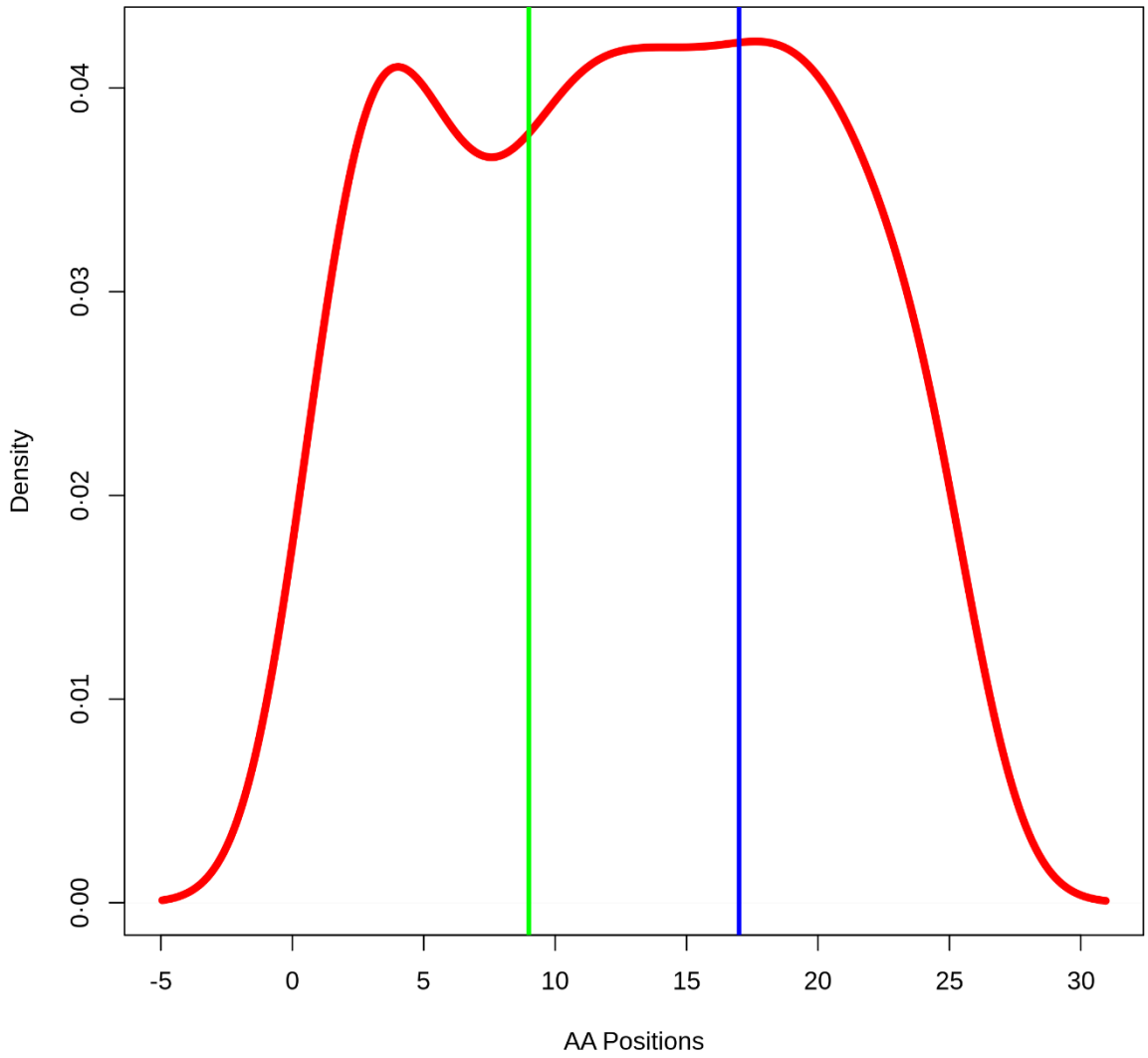

Supplementary Figure 1B: Distribution of differential cleavage sites between wild-type and mutant sequences.

Suppl. figure 1B shows the density of differences in cleavage sites between wild-type and mutant sequences. Novel cleavage site are relatively equally distributed within the whole epitope as well as the flanking regions. Only, the transition area between the N-terminal flank and the actual epitope start (aa3-aa10) seems to be less often affected than the rest.

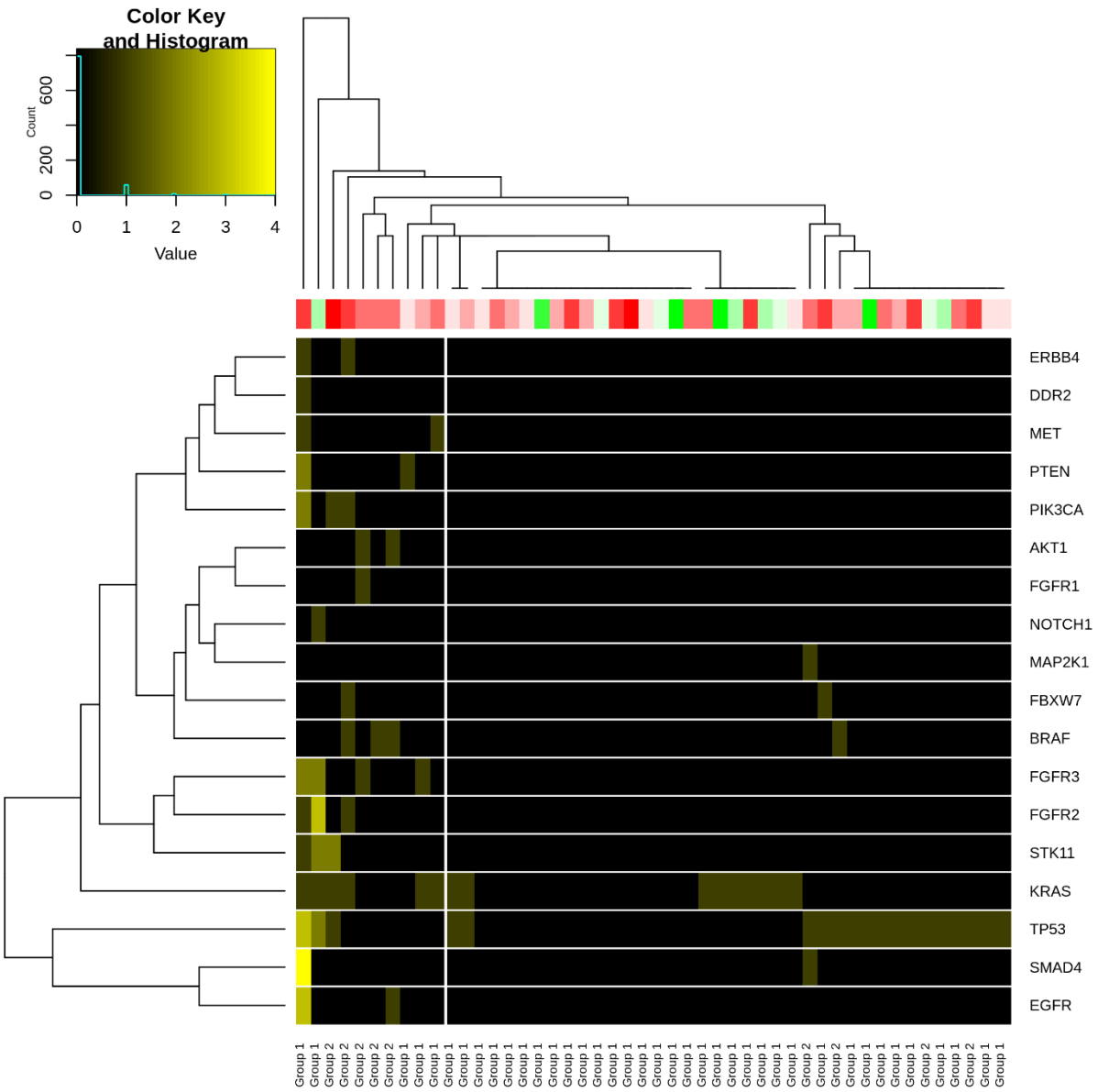

Supplementary Figure 2A: Heatmap of overall mutation load within all I/O treated samples.

The graphics illustrates unsupervised clustering of the appearance and amount of genetic variants (shown by rising intensity of yellow) within the analyzed genes (rows) for each sample separately (columns). Overall, two major groups can be identified: One group showing multiple variants in different genes (left from the white separation line), whereas the others show no or only single mutations in few genes. The color bar above indicates the outcome of patients during immunotherapy (worse-to-best by green-to-red). The column names refer to the final grouping of the samples (group 1: no processing escapes detected, group 2: processing escapes detected).

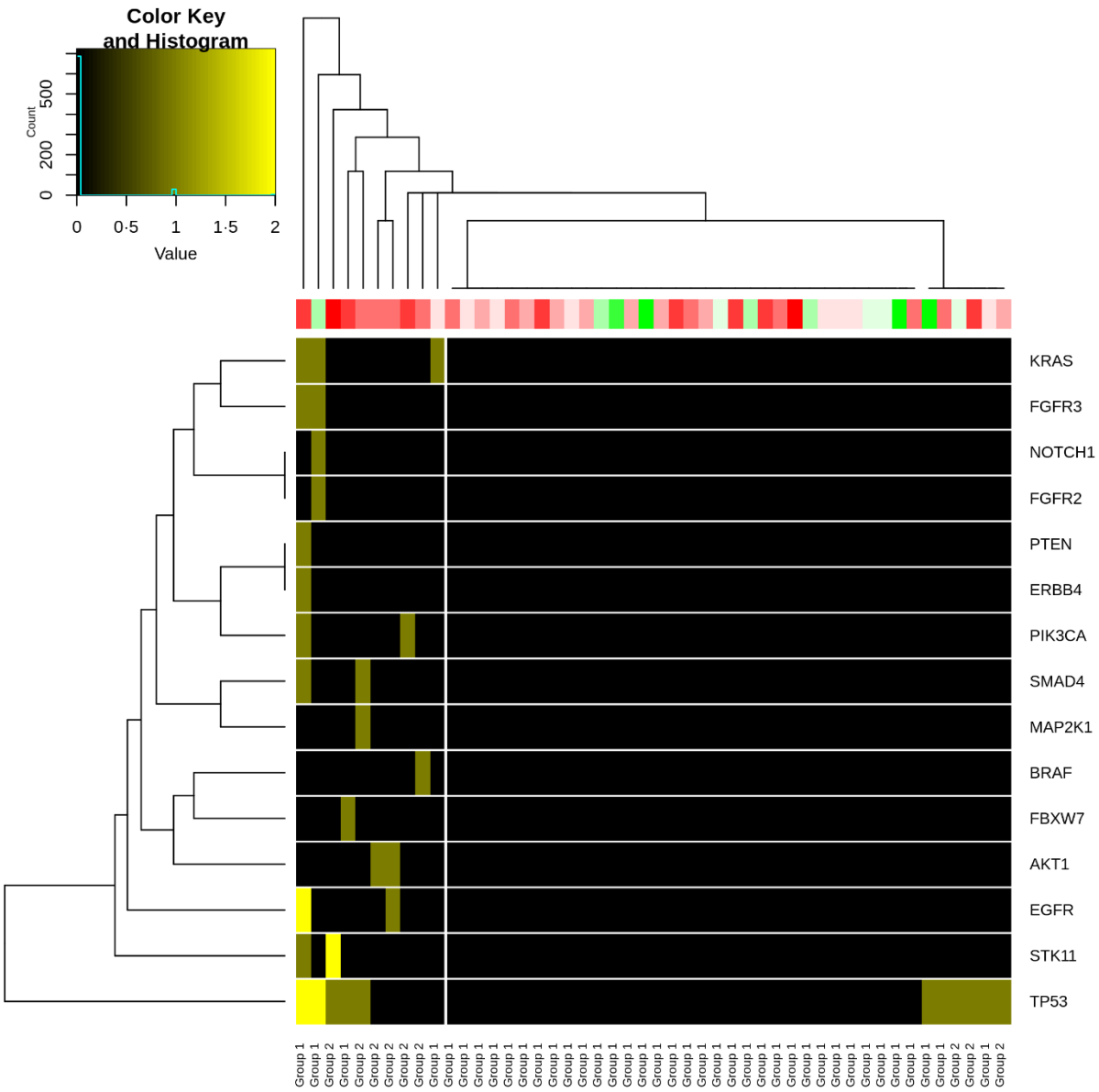

Supplementary Figure 2B: Heatmap of processing escapes within the analyzed I/O treated cohort.

The figure graphically present unsupervised clustering of the appearance and number of genetic variants associated with proteasomal immune escape (shown by rising intensity of yellow) within the analyzed genes (rows) for each sample separately (columns). Similar to overall mutation load, two major groups can be identified: One group showing processing escapes (left from the white separation line), whereas the others do not. According to the color bar indicating patient's outcome, the samples with processing escapes accumulate those with bad response, but do not exclusively comprise them all. It seems, that processing escapes reflect one but not the only important mechanism of immune escape int hose samples.

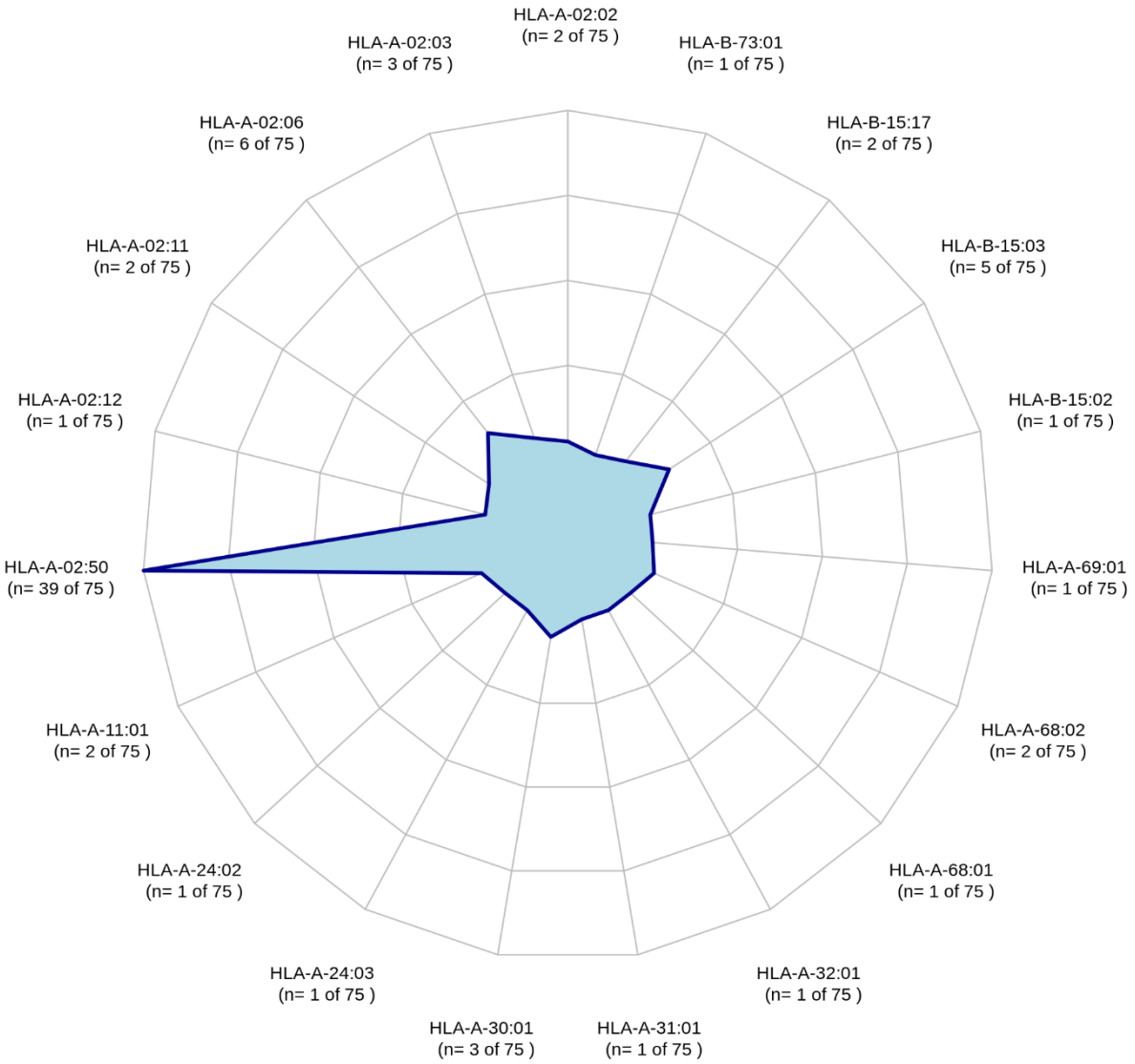

Supplementary Figure 3A: Affinity of mutated sequences not associated with processing escapes to MHC-I supertypes.

The illustration shows the binding affinities of mutated sequence-derived epitopes to MHC-I superfamilies in samples without detected processing escape mutations. Obviously, HLA-A-02:50 seems to show affinity to about half of all generated epitopes, whereas all other together comprise a minor part. Within those, HLA-A-02:06 as well as HLA-A-30:01 and HLA-B-15:03 seem to play an important role in presenting those altered fragments.

.

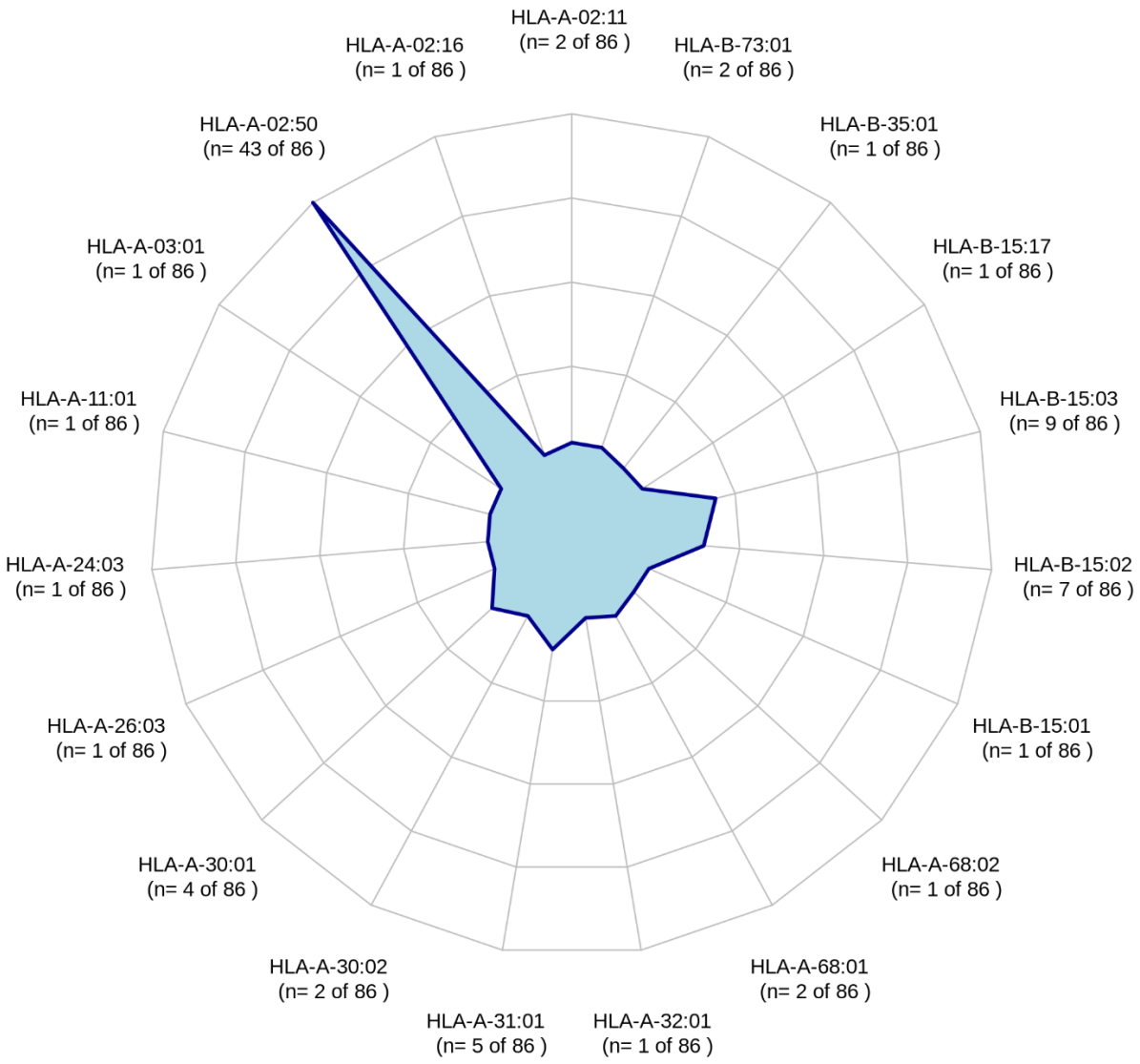

Supplementary Figure 3B: Affinity of mutated sequences associated with processing escapes to MHC-I supertypes in samples showing PD-L1 overexpression.

The illustration shows the binding affinities of mutated sequence-derived epitopes to MHC-I superfamilies in samples with the appearance of processing escape mutations combined with PD-L1 overexpression. Obviously, HLA-A-02:50 seems to show affinity to most generated epitopes, whereas all other together comprise a minor part. Within those, HLA-B-15:02, HLA-B-15:03 as well as HLA-A-31:01 and HLA-A-30:01 seem to play an important role in presenting those altered fragments.

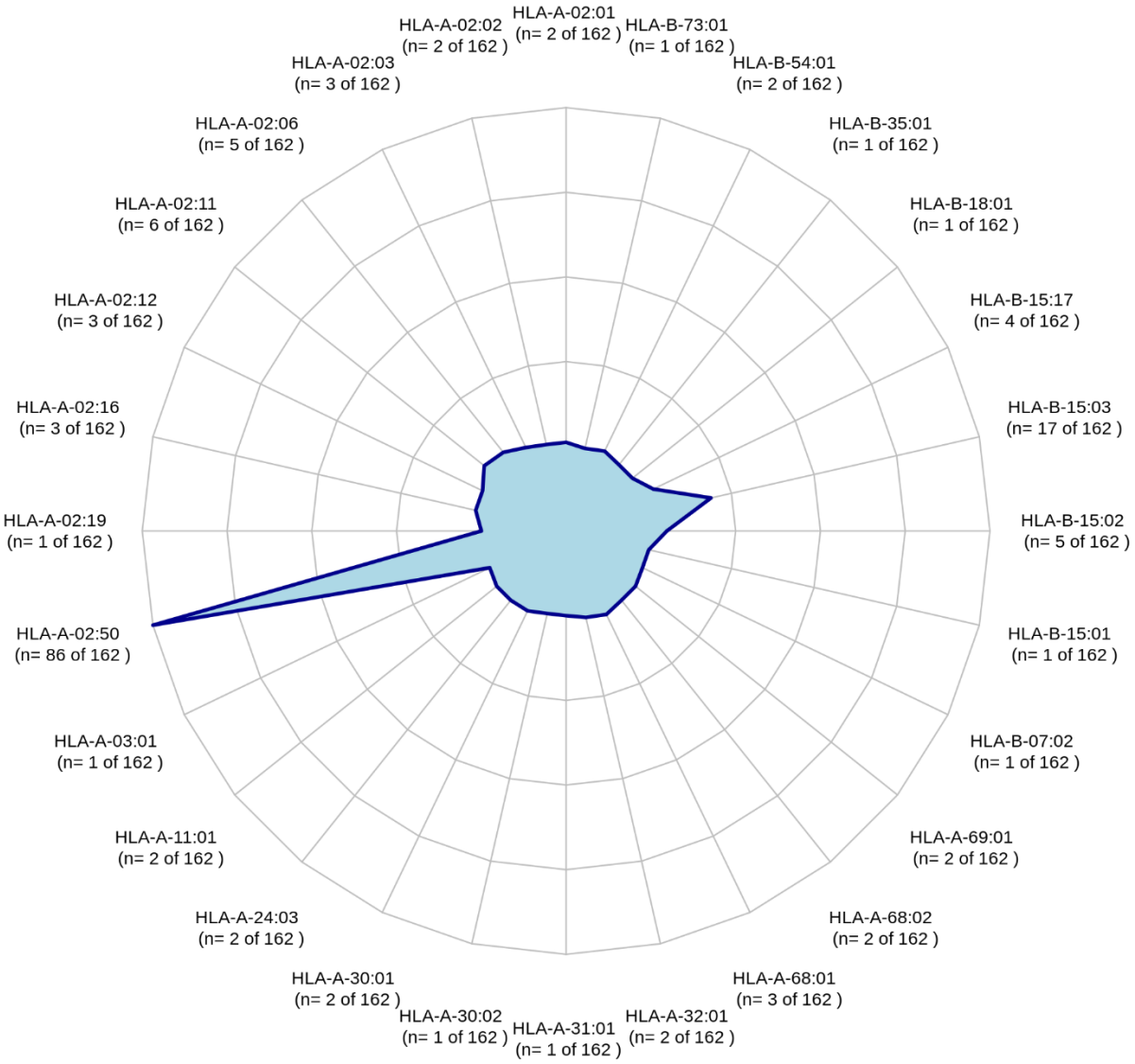

Supplementary Figure 3C: Affinity of mutated sequences associated with processing escapes to MHC-I supertypes in samples without PD-L1 overexpression.

The illustration shows the binding affinities of mutated sequence-derived epitopes to MHC-I superfamilies in samples with the appearance of processing escape mutations without an additional PD-L1 overexpression. Obviously, HLA-A-02:50 seems to again show affinity to most generated epitopes, whereas all other together comprise a minor part. Only HLA-B-15:03 seem to play an additianl role in presenting those altered fragments within this subgroup of patients.

	AKT1	BRAF	DDR2	EGFR	ERBB4	FBXW7	FGFR1	FGFR2	FGFR3	KRAS	MAP2K1	MET	NOTCH1	PIK3CA	PTEN	SMAD4	STK11	TP53
Mutational load	2	4	1	4	2	2	1	5	6	15	1	2	1	4	3	5	5	22
Processing mutations	2	1	0	2	1	1	0	1	2	3	1	0	1	2	1	2	2	10

Supplementary Figure 4A: Distribution of mutations across affected genes.
The spider plots show genes (n=18) mostly affected by non-synonymous mutations (“Mutational Load”, green) in the current NSCLC cohort. The most affected gene was TP53 (n= 22) followed by KRAS (n=). Other candidates include NOTCH1, BRAF, EGFR, as well as FGFR3/2. Part of those mutations were also affecting proteasomal processing (“Processing escape mutations”, red). While TP53 still has most of the mutations influencing proteasomal processing (n= 9), the amount of mutations in KRAS (n=), BRAF, MET was decreasing. Which means fewer of those mutations influence proteasomal processing. All in all, the mutational distribution between both groups does not differ much.

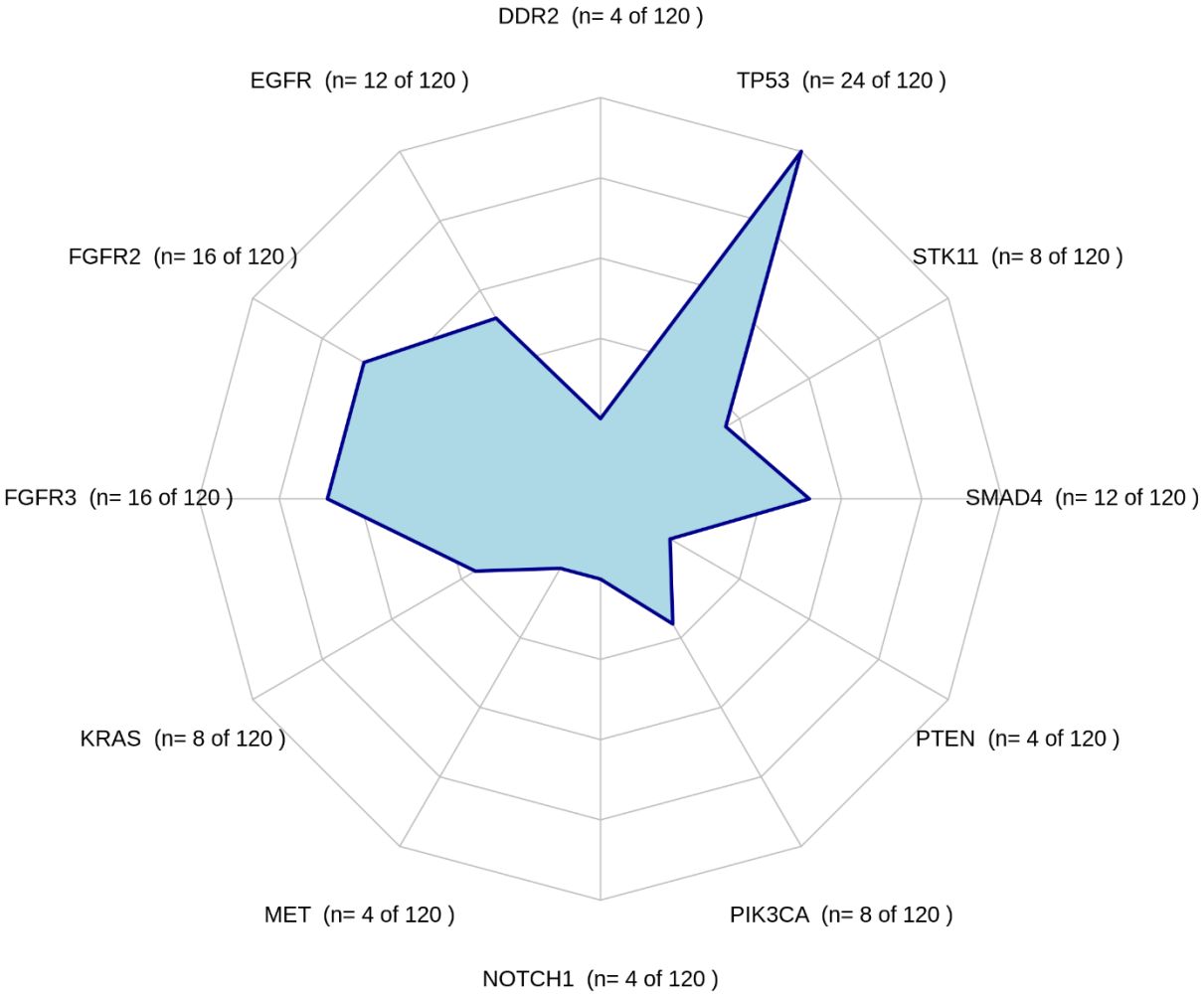

Supplementary Figure 4B: Distribution of genes affected by mutations not associated with processing escapes.

Suppl. figure 4A illustrates the spreading of passenger mutations between different gene loci. The mostly affected gene is *TP53*, followed by *FGFR2* as well as *FGFR3*, *EGFR* as well as *SMAD4*, *KRAS* as well as *PIK3CA* as well as *STK11* and *DDR2* as well as *PTEN* as well as *NOTCH1* as well as *MET*.

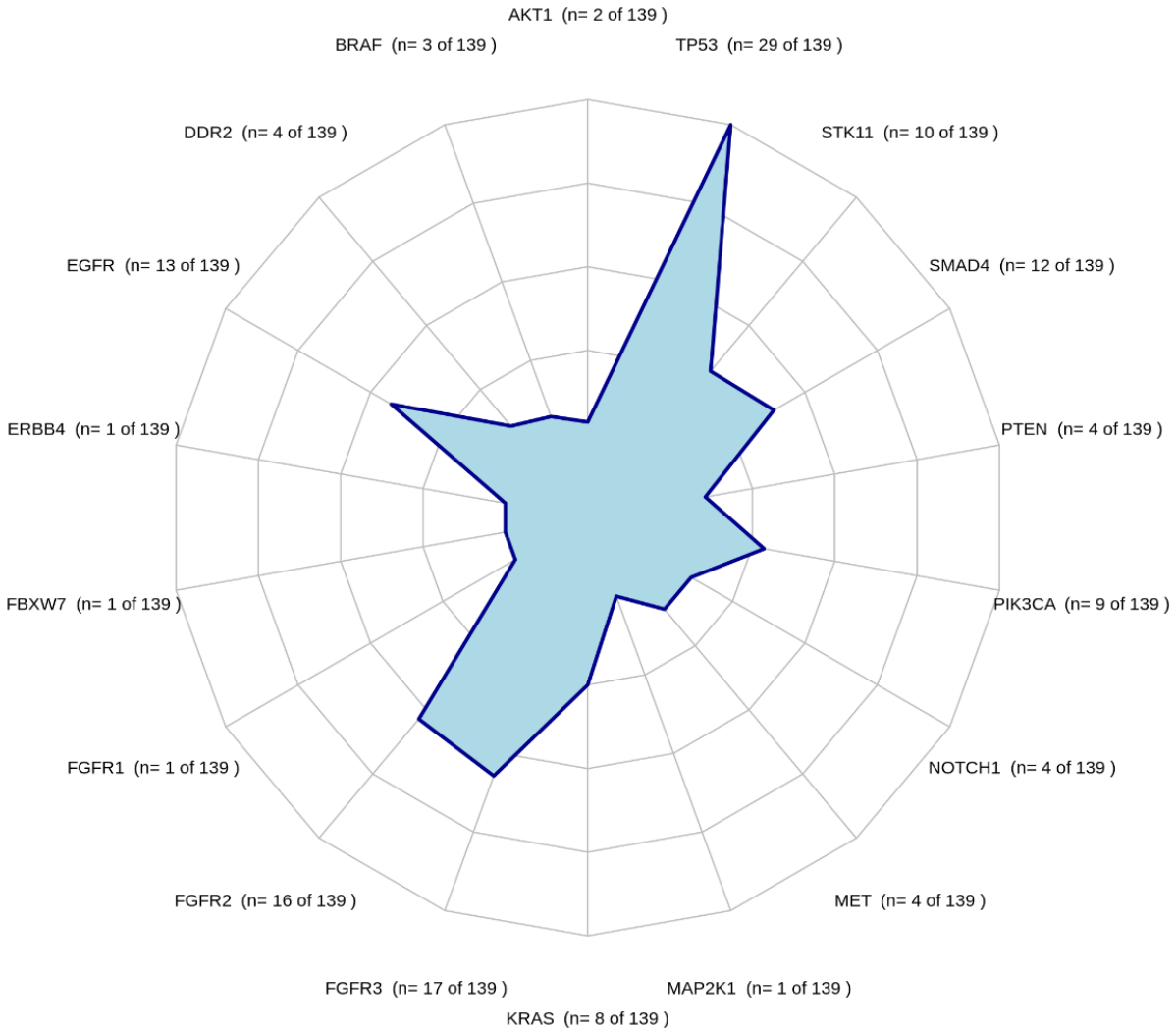

Supplementary Figure 4C: Distribution of genes affected by mutations associated with processing escapes in samples showing PD-L1 overexpression. Suppl. figure 4A illustrates the spreading of passenger mutations between different gene loci. The mostly affected gene is *TP53*, followed by *FGFR3, FGFR2*, *SMAD4 and STK11*. For the remaining 17 genes, only few (*AKT1, PTEN, PIK3CA, NOTCH1, MET, KRAS, DDR2, BRAF*) or single (*MAP2K1, FGFR1, FBXW7, ERBB4*) variations could be detected.

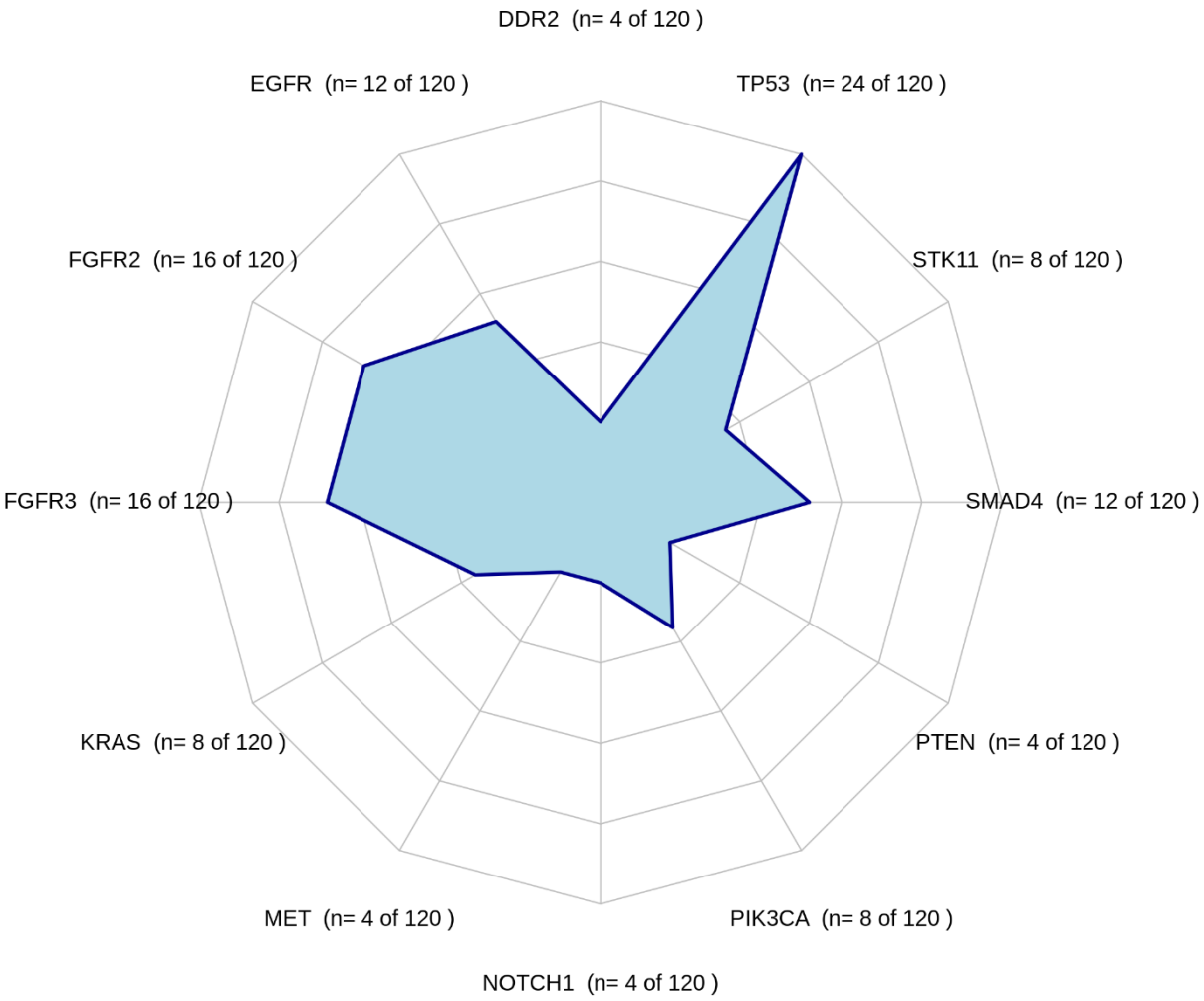

Supplementary Figure 4D: Distribution of genes affected by mutations associated with processing escapes in samples without PD-L1 overexpression. Suppl. figure 4A illustrates the spreading of passenger mutations between different gene loci. Comparably with the gene distribution from the group of samples without showing processing escapes, the mostly affected gene is *TP53*, followed by *FGFR2* as well as *FGFR3*, *EGFR* as well as *SMAD4*, *KRAS* as well as *PIK3CA* as well as *STK11* and *DDR2* as well as *PTEN* as well as *NOTCH1* as well as *MET*.

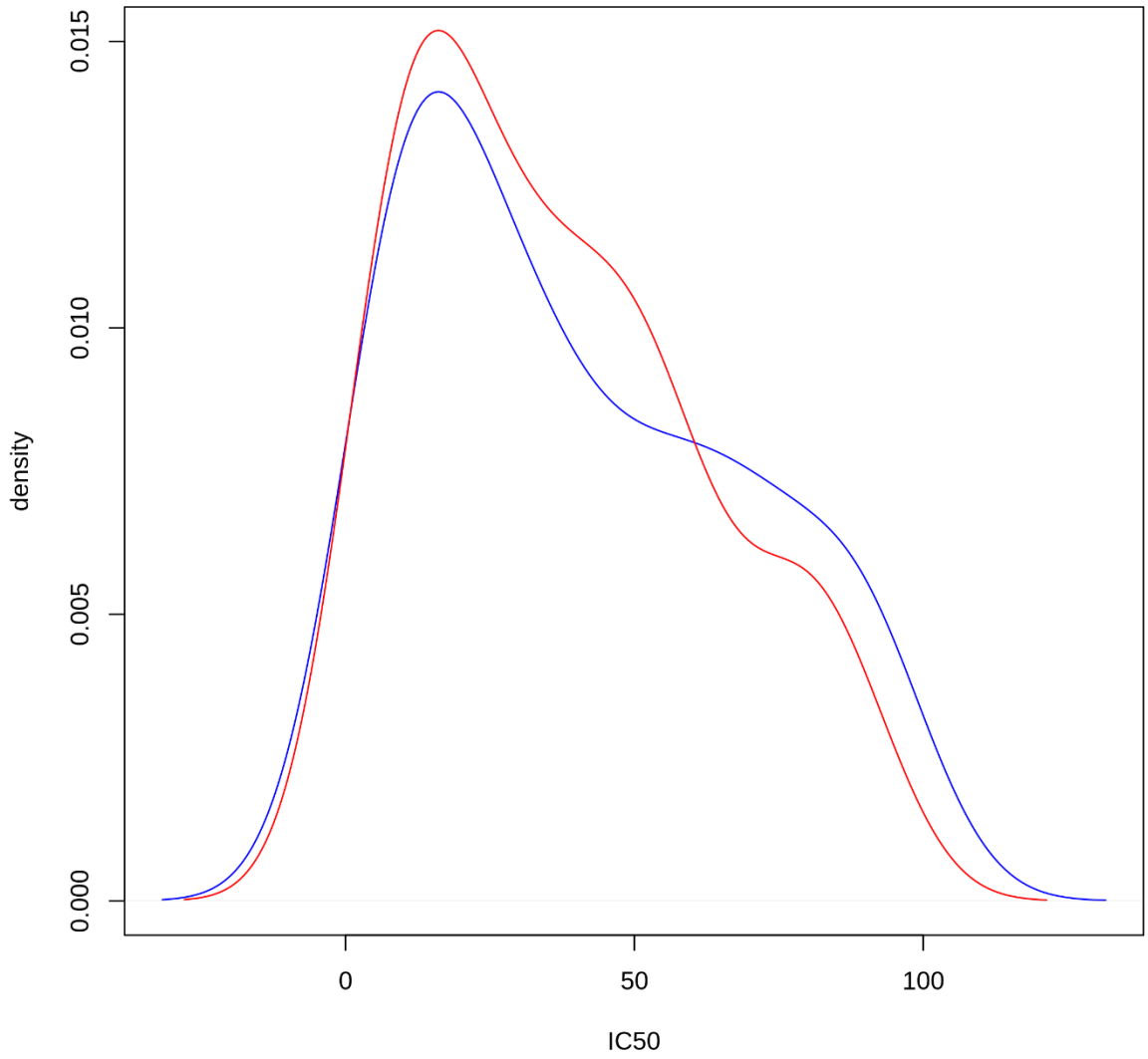

Supplementary Figure 5A: Binding affinity of mutated sequences not associated with processing escapes to MHC-I supertypes.
Suppl. figure 5A shows a density plot of IC50 values of binding affinities to MHC-I of all analyzed epitopes. The red line indicates epitopes derived from mutated sequences; the blue line indicates epitopes derived from wild-type sequences. For mutations not associated with proteasomal processing, altered epitopes overall show elevated binding affinity compared to their wild-type counterparts. This indicates presentation of the derived neoantigens to the hosts immune system.

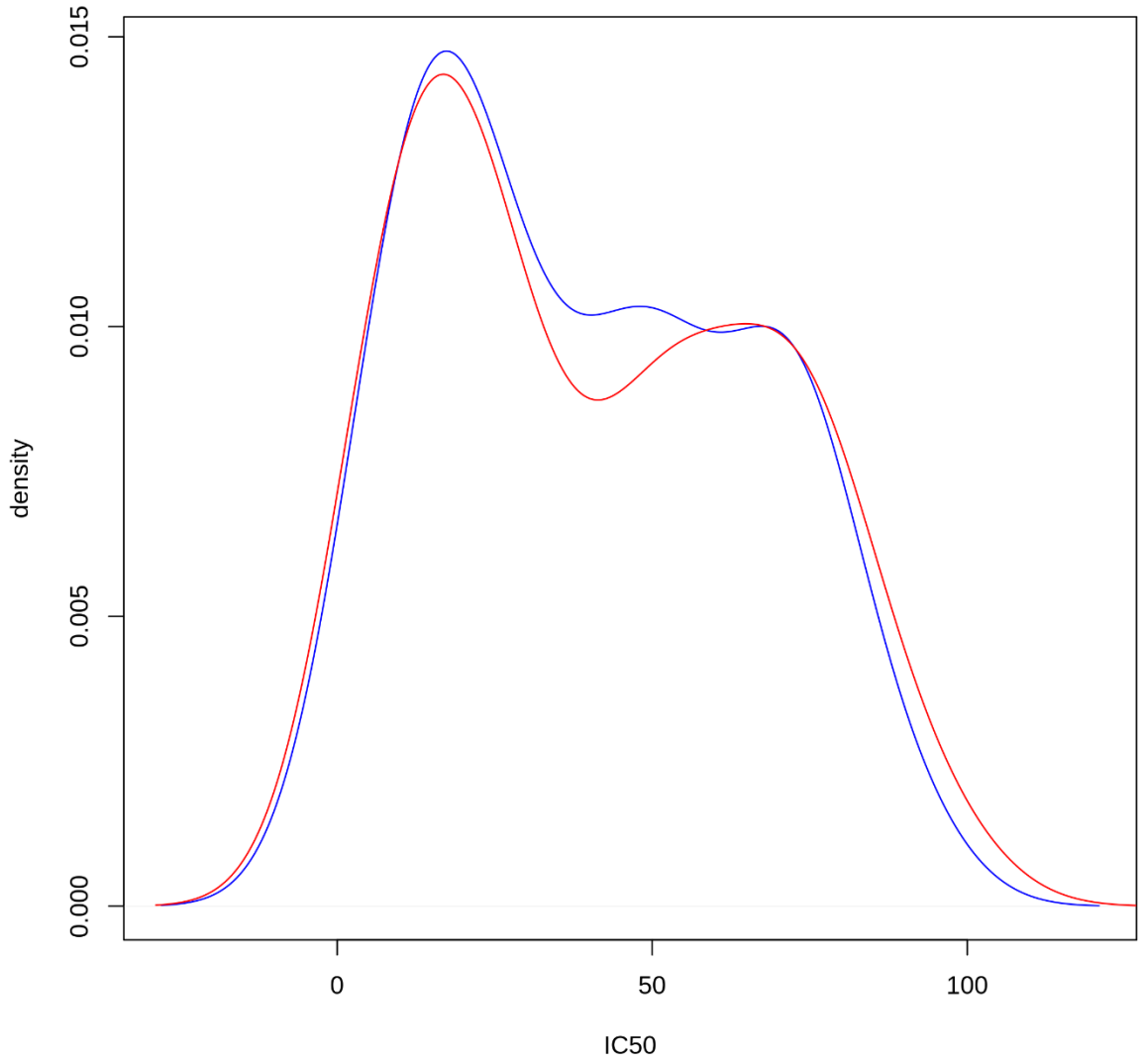

Supplementary Figure 5B: Binding affinity of mutated sequences associated with processing escapes to MHC-I supertypes in samples showing PD-L1 overexpression.

Suppl. figure 5B shows a density plot of IC50 values of binding affinities to MHC-I of all analyzed epitopes. The red line indicates epitopes derived from mutated sequences; the blue line indicates epitopes derived from wild-type sequences. For mutations associated with proteasomal processing in tumors with simultaneous PD-L1 overexpression, especially those epitopes with borderline binding (IC50 between 30 to 60) show a significantly reduced binding on the cell surface compared to their wild-type counterparts. This indicates clearly reduced presentation of the derived neoantigens on the cell surface and subsequently decreased potential for activation of hosts immune system.

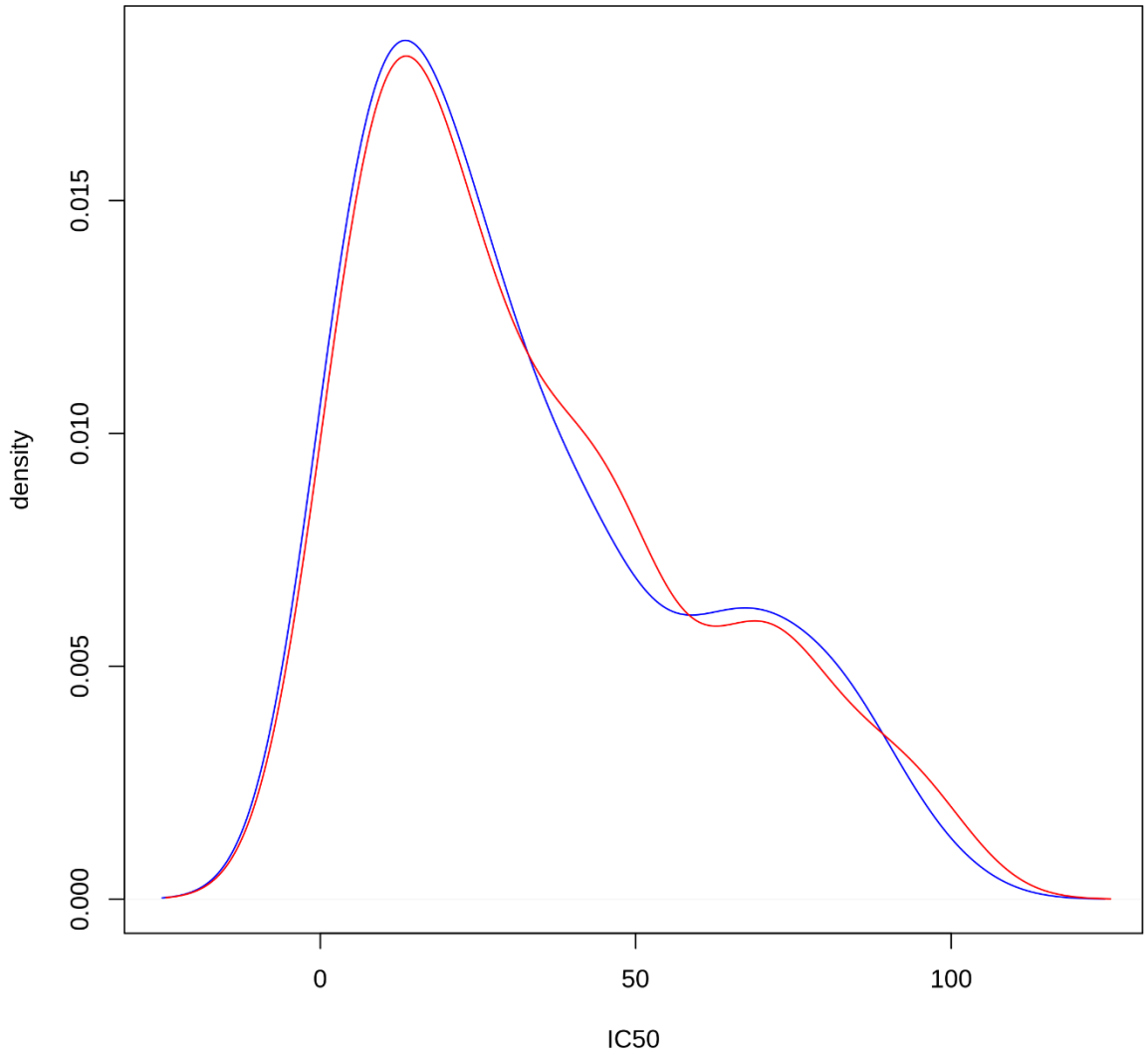

Supplementary Figure 5C: Binding affinity of mutated sequences associated with processing escapes to MHC-I supertypes in samples without PD-L1 overexpression.

The density plot illustrates IC50 values of binding affinities to MHC-I of all analyzed epitopes. The red line indicates epitopes derived from mutated sequences; the blue line indicates epitopes derived from wild-type sequences. For mutations associated with proteasomal processing in tumors without simultaneous PD-L1 overexpression, contrarily to those samples showing an additional PD-L1 expression, no significant difference between wild-type and altered fragments regarding their binding intensity could be observed. In this group of samples, a presentation of the alteren epitopes is still likely to occur.

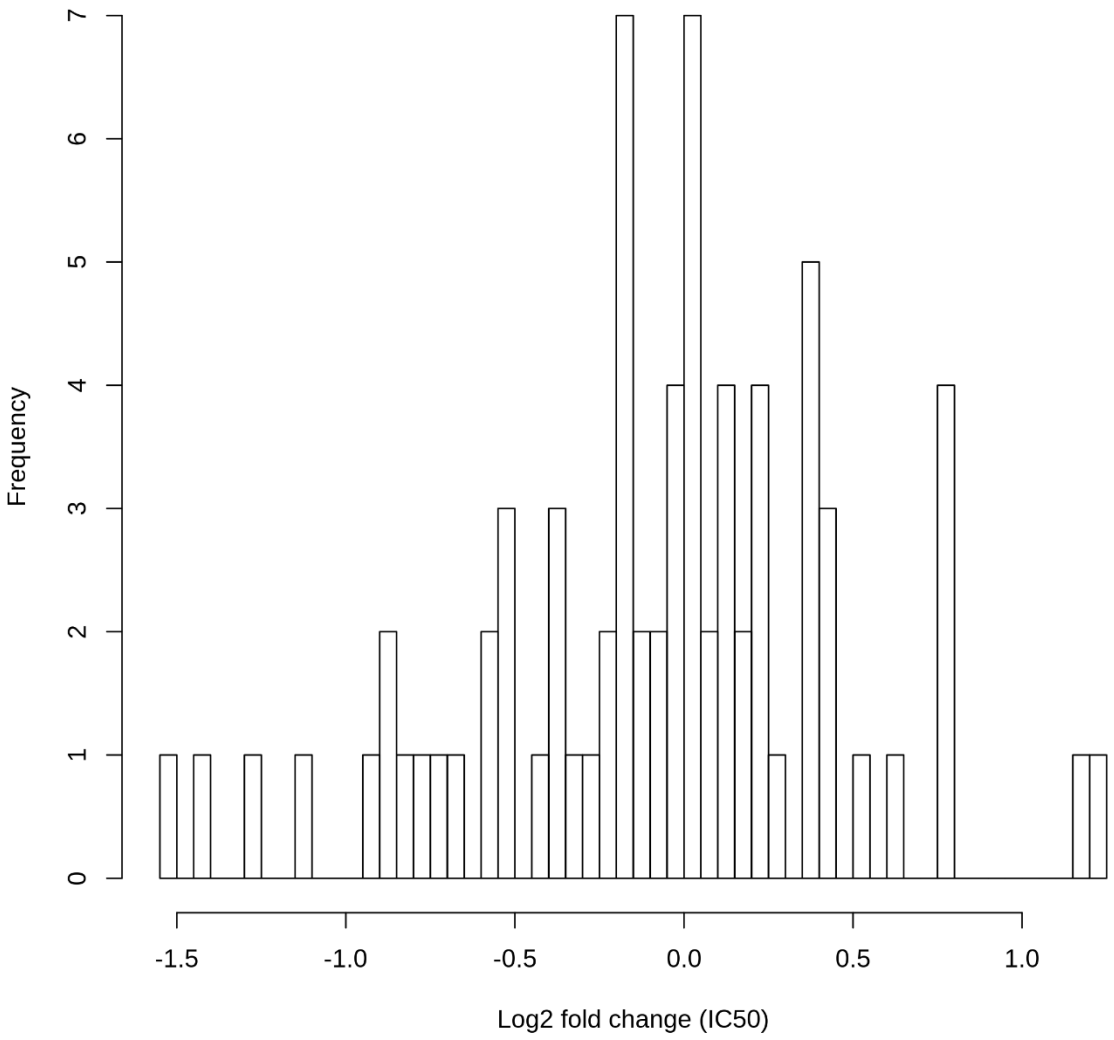

Supplementary Figure 6A: Difference between wild-type and mutant epitope pair in their binding affinity to MHC-I molecules in samples showing no variants associated with proteasomal immune escapes

The figure illustrates a histogram plotting the difference of MHC-I binders in binding affinity estimates as IC50 values. The x-axis depicts the log2-fold change between mutant and wild-type derived epitopes from the same sequences as pairs. Two-third of neoepitopes in samples without proteasomal processing escape associated mutations seem to have the same or a stronger affinity compared to their counterparts, which reflects our hypothesis of an intact presentation of neoantigen in those cells.

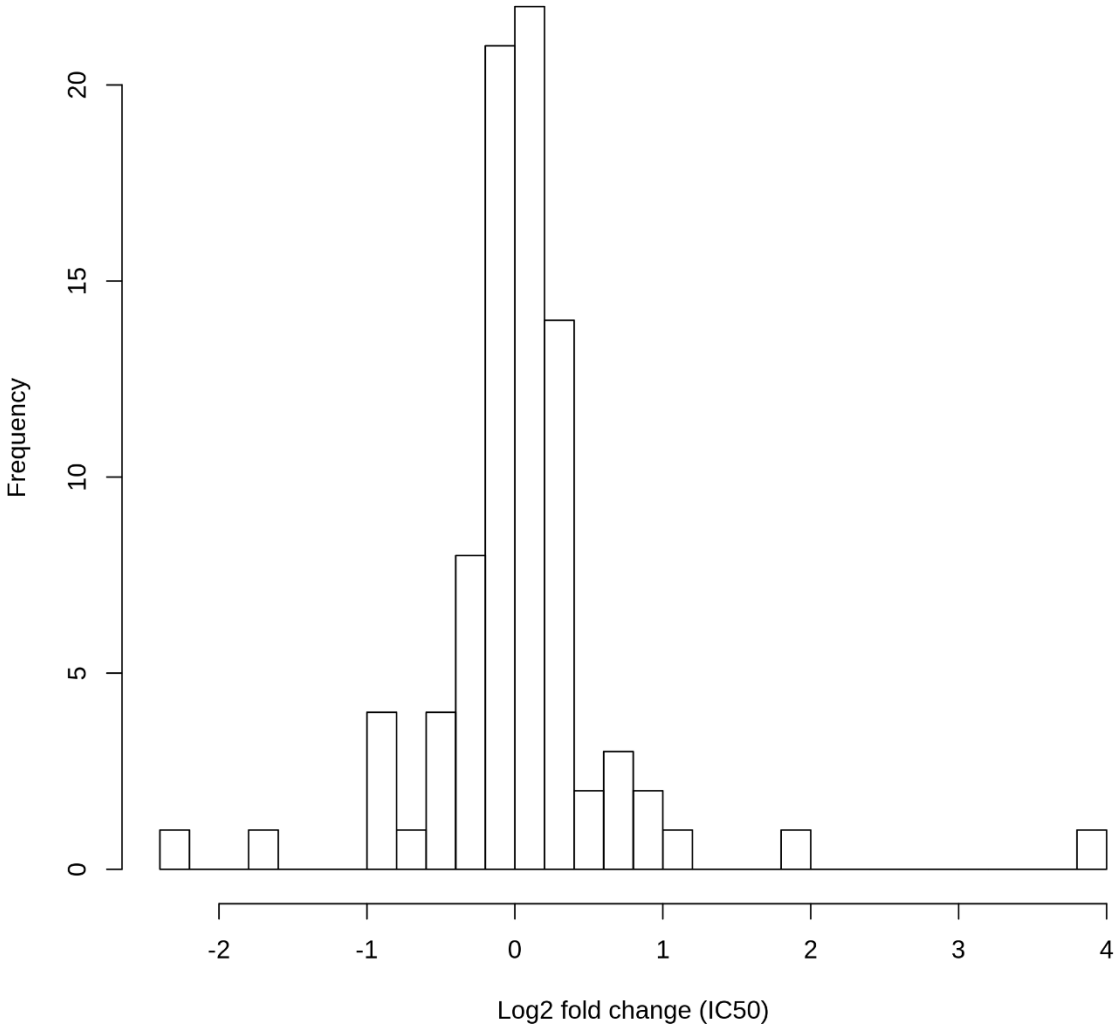

Supplementary Figure 6B: Difference between wild-type and mutant epitope pair in their binding affinity to MHC-I molecules in samples showing variants associated with proteasomal immune escapes and additional PD-L1 overexpression.

The figure illustrates a histogram plotting the difference of MHC-I binders in binding affinity estimates as IC50 values. The x-axis depicts the log2-fold change between mutant and wild-type derived epitopes from the same sequences as pairs. The majority of neoepitopes from proteasomal processing escape associated mutations in sanmples with PD-L1 overexpression show reduced affinity to MHC-I molecules compared to their counterparts, indicating a reduced or lost presentation of those to the hosts immune system.

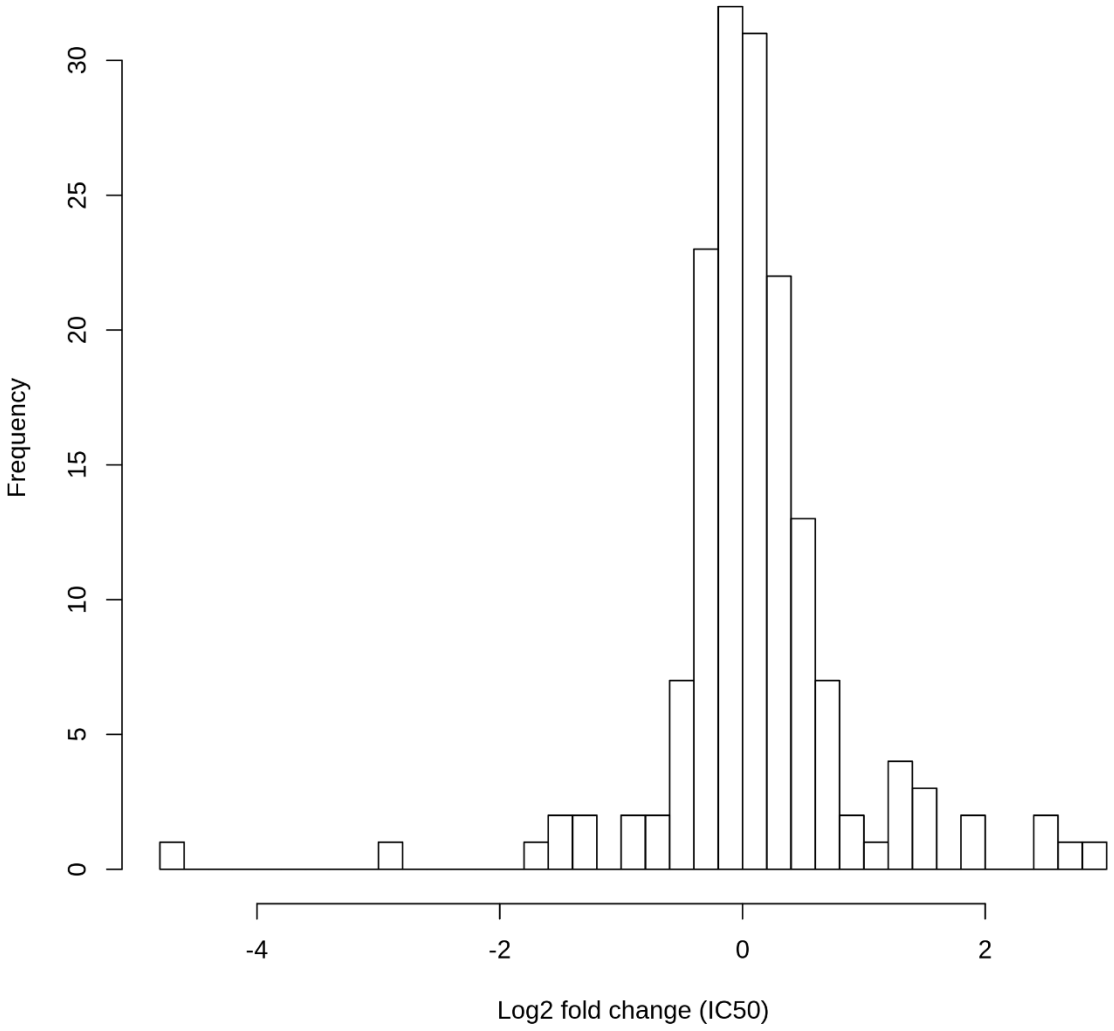

Supplementary Figure 6C: Difference between wild-type and mutant epitope pair in their binding affinity to MHC-I molecules in samples showing variants associated with proteasomal immune escapes without additional PD-L1 overexpression.

The figure illustrates a histogram plotting the difference of MHC-I binders in binding affinity estimates as IC50 values. The x-axis depicts the log2-fold change between mutant and wild-type derived epitopes from the same sequences as pairs. The majority of neoepitopes from proteasomal processing escape associated mutations in sanmples without PD-L1 expression show slightly reduced affinity to MHC-I molecules compared to their counterparts, indicating a reduced or lost presentation of those to the hosts immune system similar to those in samples with PD-L1 expression.

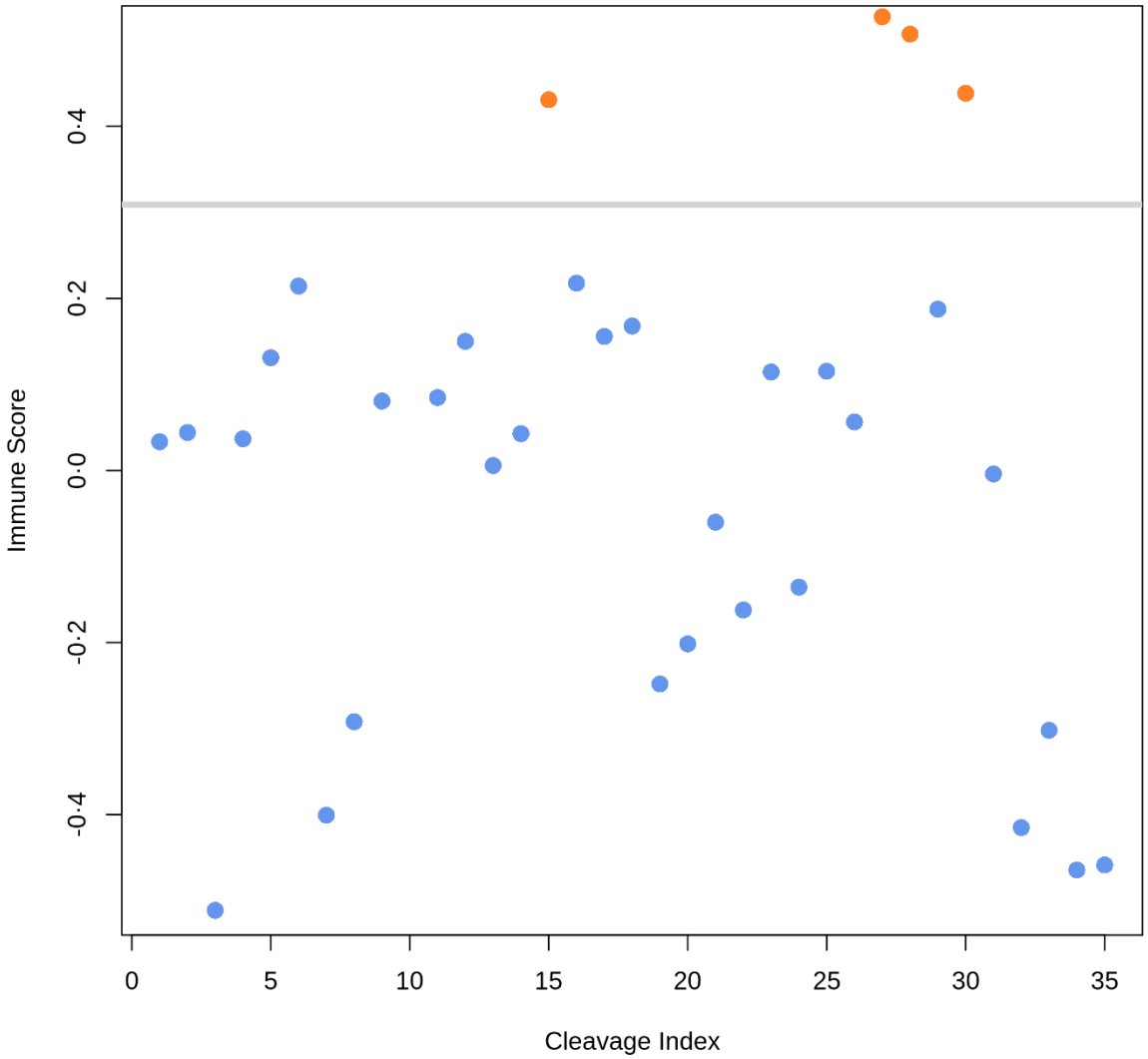

Supplementary Figure 7: Influence of cleavage position within the epitope/flanking region on immunogenicity of the resulting neoepitope for proteasomal processing escape mutations.
The graphics illustrates the influence of aa position of an additional proteasomal cleavage within the epitope including the flanking region to the potency of activating hosts T-cell response by the resulting neoepitope. Only a few single variants show the potential to somehow activate hosts anti-cancer immune defense. On the other hand, the vast majority has not been predicted to somehow trigger any immunoreaction.

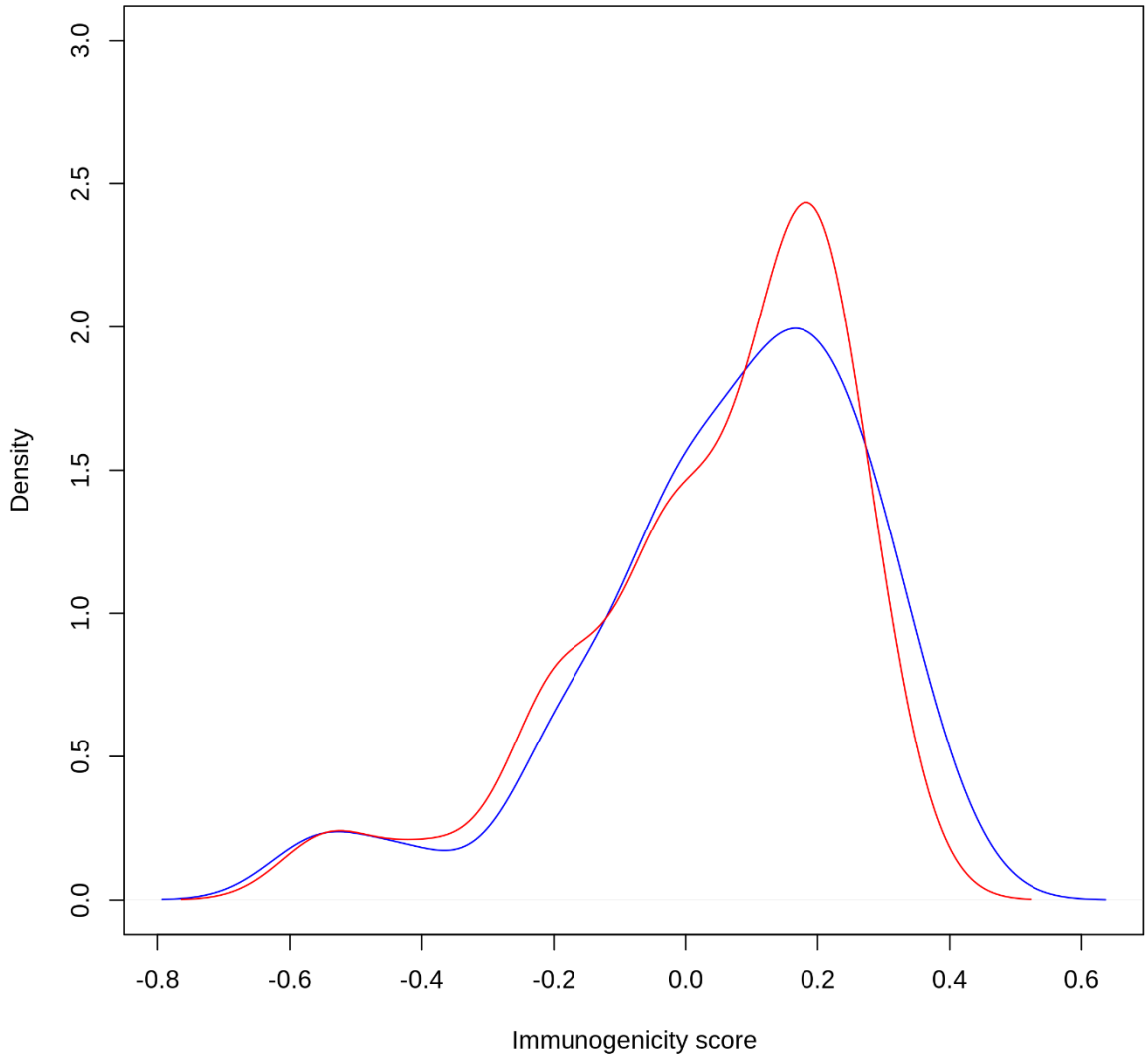

Supplementary Figure 8A: Immunogenicity in wild-type and neoantigen derived epitopes in tumors showing no variants associated with proteasomal immune escapes.

The figure depicts a density plot of immunogenicity scores of all analyzed epitopes. The red line indicates epitopes derived from mutated sequences; the blue line indicates epitopes derived from wild-type sequences. Negative values refer to a stronger potency of immunoactivation, whereas positive values do not. For mutations not associated with proteasomal processing, resulting epitopes show a similar distribution of activating epitopes, compared to the wild type (peak between -0.6 and -0.4). Overall, a slight shift to the left can be seen for mutation-derived epitopes, indicating an overall stronger signal for T-cell activation

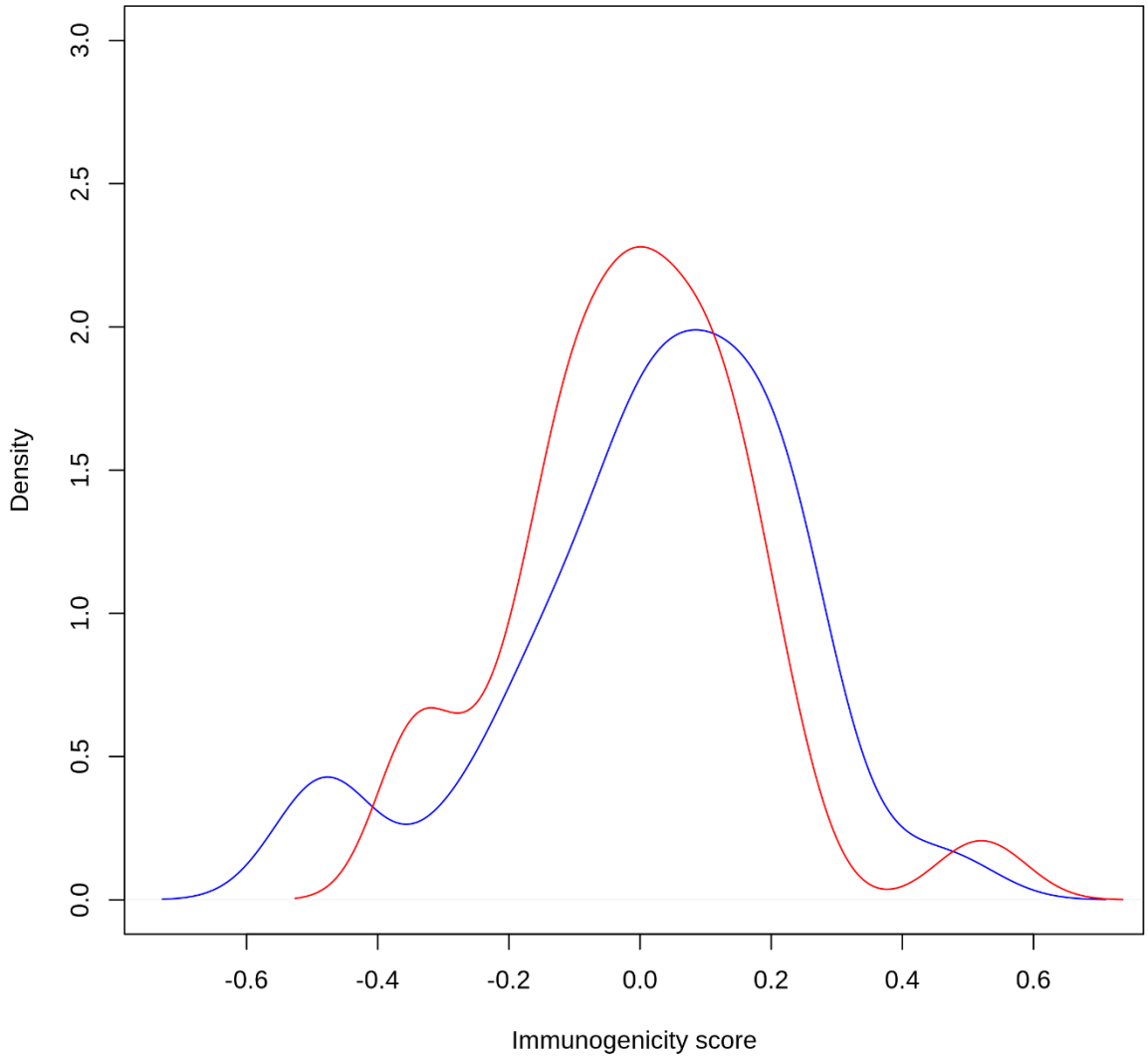

Supplementary Figure 8B: Immunogenicity in wild-type and neoantigen derived epitopes in tumors showing variants associated with proteasomal immune escapes and additional PD-L1 overexpression.

The figure depicts a density plot of immunogenicity scores of all analyzed epitopes. The red line indicates epitopes derived from mutated sequences; the blue line indicates epitopes derived from wild-type sequences. Negative values refer to a stronger potency of immunoactivation, whereas positive values do not. For variants resulting in proteasomal processing immune-escapes, resulting epitopes show a differing distribution of activating epitopes compared to the wild type. Whereas the wild-type derived epitopes show a clear peak in the immune-activating region (left), this peak is shifted more to the range between -0.4 and -0.2, which leads to strongly reduced immune recognition. On the other hand, a distinct peak between 0.4 and 0.6 can be seen, presenting epitopes that are clearly not able to trigger TCR-based signals. Summing up, neoantigens in patients with processing escapes and additional PD-L1 overexpression are less potent to activate hosts immune system.

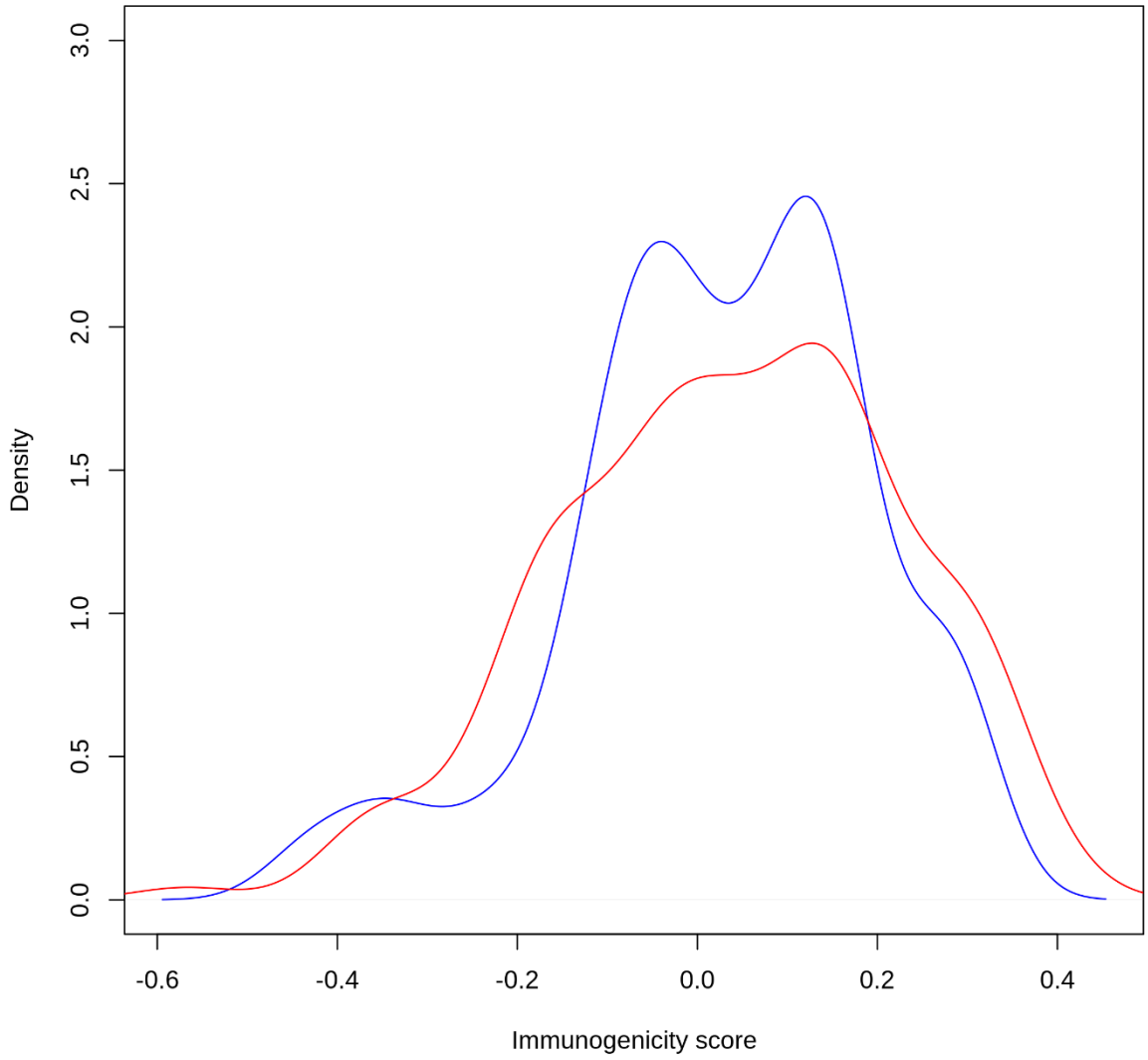

Supplementary Figure 8C: Immunogenicity in wild-type and neoantigen derived epitopes in tumors showing variants associated with proteasomal immune escapes without PD-L1 overexpression.

The figure depicts a density plot of immunogenicity scores of all analyzed epitopes. The red line indicates epitopes derived from mutated sequences; the blue line indicates epitopes derived from wild-type sequences. Negative values refer to a stronger potency of immunoactivation, whereas positive values do not. For variants resulting in proteasomal processing immune-escapes, generated epitopes show no a clear peak in the immune-activating region (left) compared to the wild-type samples. Overall, the curve looks swaged with some neoepitopes slightly enhance tumors immunogenicity without reaching the point to trigger a real anti-cancer immune reaction, but also shift the overall values more to the right, leading to overall more invisibility of the cell to hosts immune system. Summing up, neoantigens in patients with processing escapes without PD-L1 overexpression seem to less potent to activate hosts immune system, however this effect seems not as strong as it is with an additional PD-L1 overexpression.

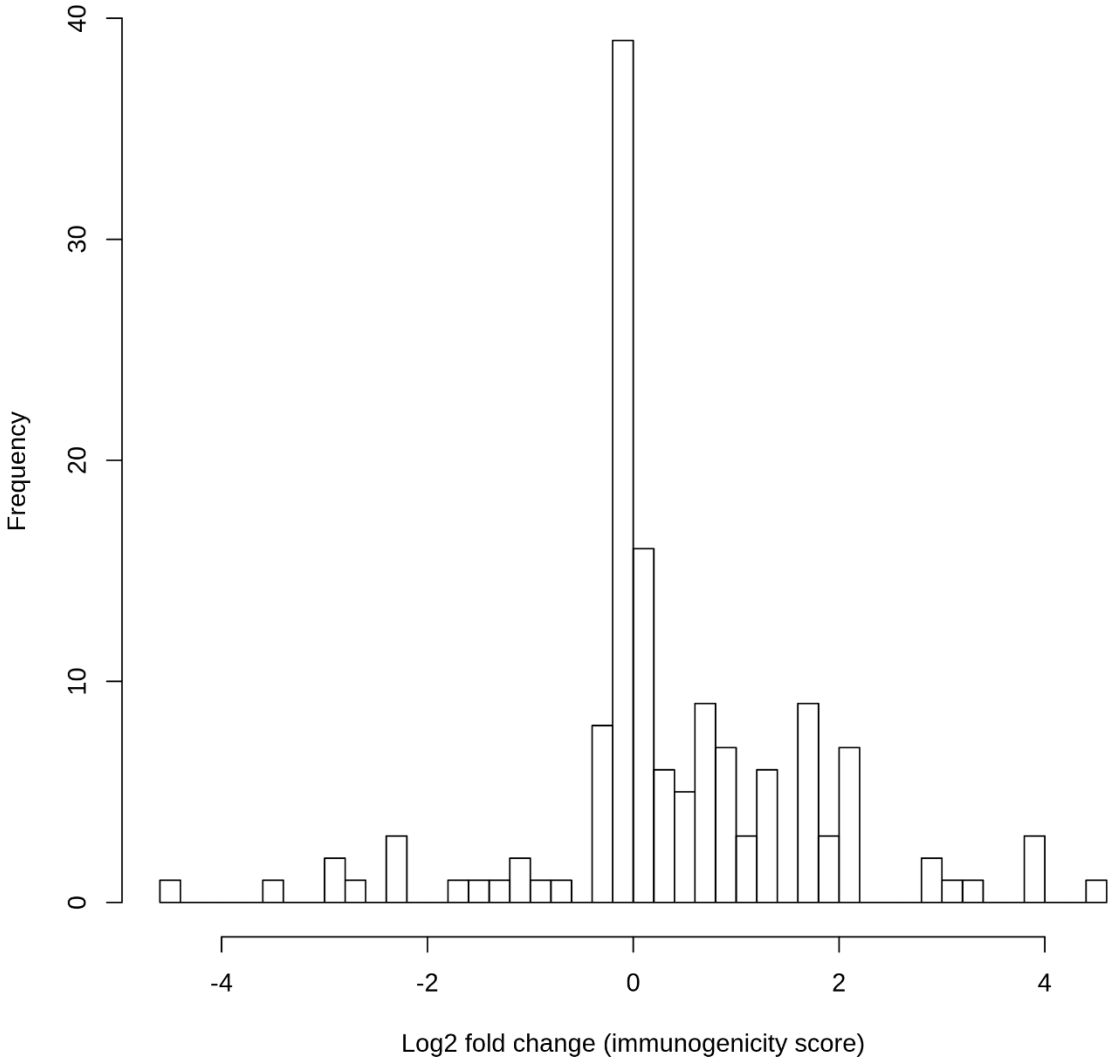

Supplementary Figure 9A: Relative difference in immunogenicity between wild-type and neoantigen derived epitopes in tumors showing no variants associated with proteasomal immune escapes.

The histogram illustrates the log2 fold change of the potency to trigger T-cell based host's immune reaction between mutant epitopes compared with their wild-type counterparts. Negative values indicate an enhanced, positive values a lowered immunoreactivity potential. In samples showing no variants associated with altered proteasomal epitope processing, the majority of epitopes will not trigger an anti-cancer immune response. Nevertheless, there is a substantial proportion of fragments that can induce a potent activation of the immune system. This underlines our hypothesis, that in those cases there are neoantigens of good quality, and that there is a potential of re-activation of hosts anti-cancer immune response.

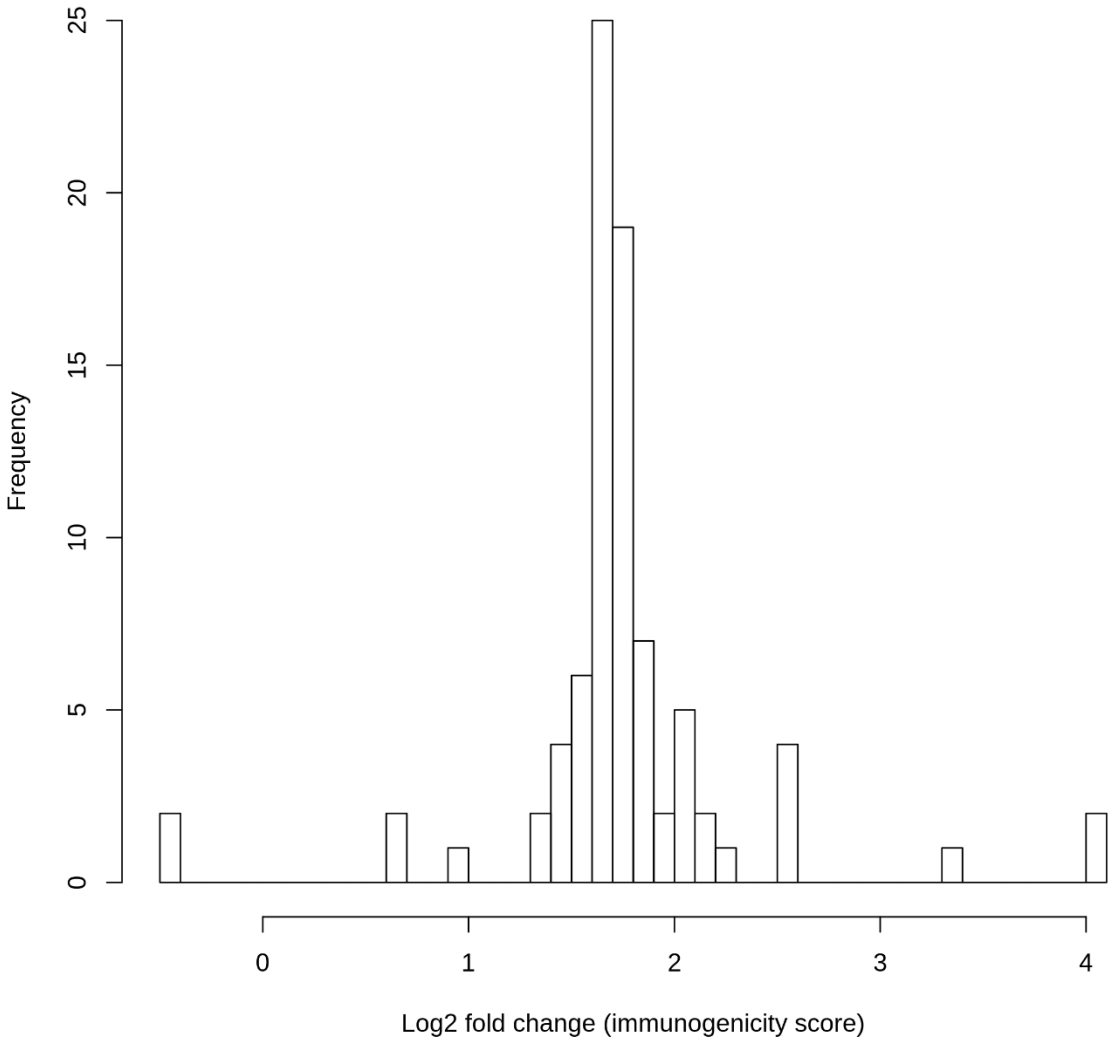

Supplementary Figure 9B: Relative difference in immunogenicity between wild-type and neoantigen derived epitopes in tumors showing variants associated with proteasomal immune escapes and additional PD-L1 overexpression.
The histogram illustrates the log2 fold change of the potency to trigger T-cell based host's immune reaction between mutant epitopes compared with their wild-type counterparts. Negative values indicate an enhanced, positive values a lowered immunoreactivity potential. In tumors showing variants associated with proteasomal immune escapes and additional PD-L1 overexpression, the epitopes derived from mutant sequences nearly exclusively lower epitopes immunogenicity, underlying the importance of this mechanism to shut down hosts immune system.

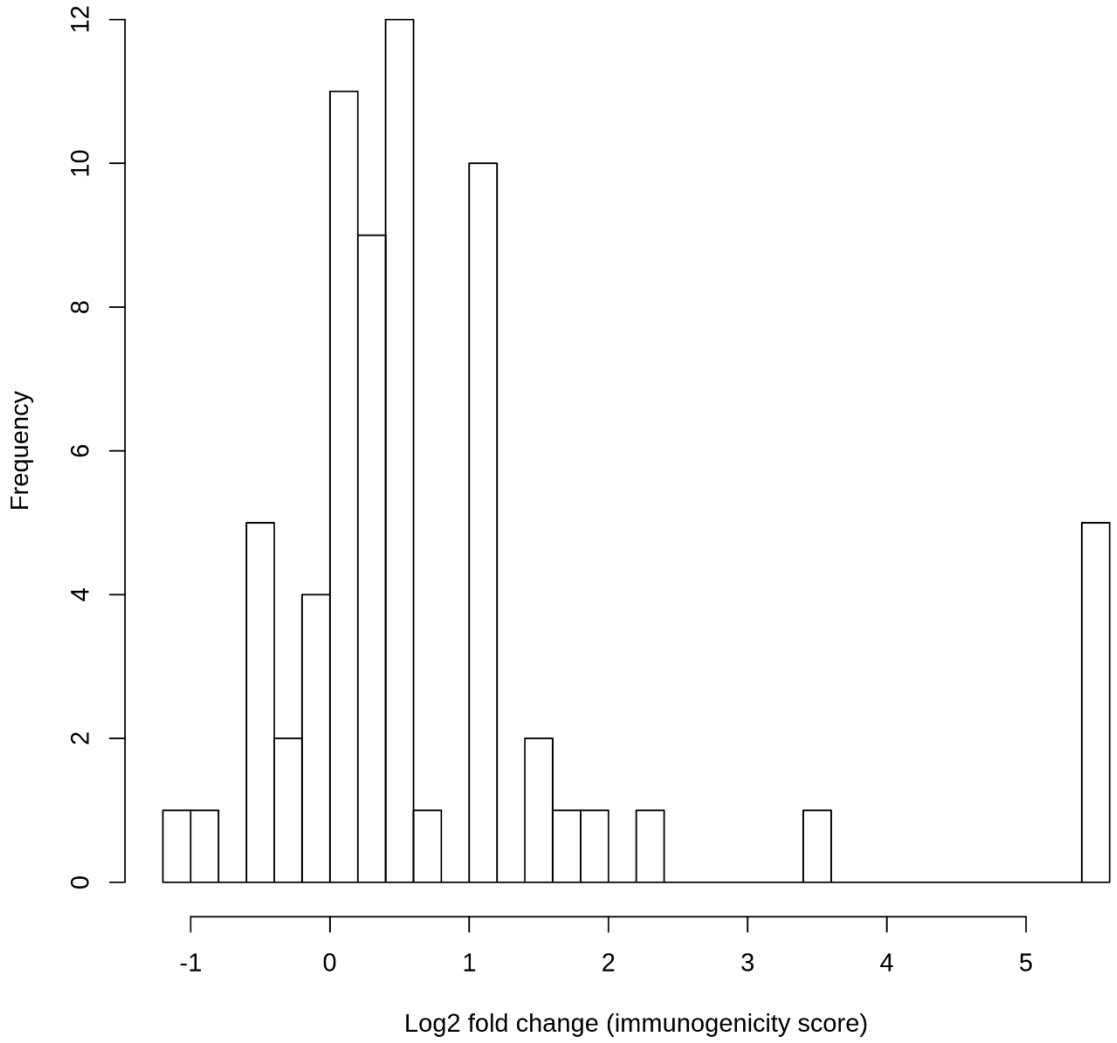

Supplementary Figure 9C: Relative difference in immunogenicity between wild-type and neoantigen derived epitopes in tumors showing variants associated with proteasomal immune escapes without PD-L1 overexpression.

The histogram illustrates the log2 fold change of the potency to trigger T-cell based host's immune reaction between mutant epitopes compared with their wild-type counterparts. Negative values indicate an enhanced, positive values a lowered immunoreactivity potential. In tumors showing variants associated with proteasomal immune escapes without PD-L1 expression, overwhelming majority of epitopes derived from mutant sequences significantly lower hosts ability of an intact immune response. However, there are some fragments that are potentially increase cells immunogenicity and thereby the potential of activating TCR signaling, these effects are much weaker then seen in samples showing no variants associated with altered proteasomal epitope processing. Even when resulting in an overall reduced immune reactivity against these cancers, there may be the potential of a therapeutic restore of T-cell activity.

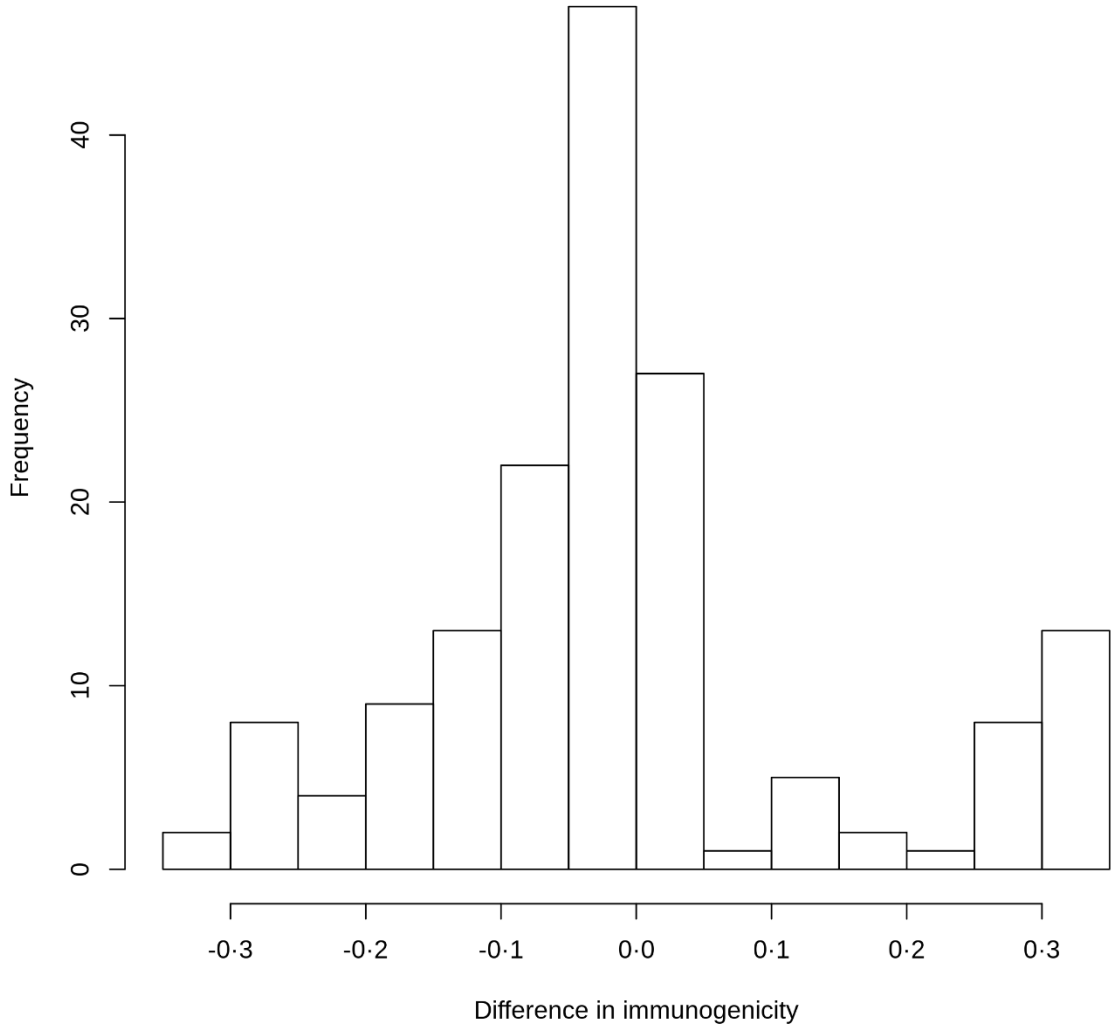

Supplementary Figure 10A: Absolute difference in immunogenicity between wild-type and neoantigen derived epitopes in tumors showing no variants associated with proteasomal immune escapes

The histogram illustrates the absolute differences in the immunogenicity between epitopes derived from mutant sequences compared to those derived from their wild-type counterparts in cases without processing escapes. Negative values indicate an enhanced, positive values a lowered potential of activating the immune system. A gross of mutant epitopes only slightly enhance or do not affect immunogenic potential. However, there is a significant number of epitopes which enhance the immunogenic potential of those. Also, some epitopes significantly decrease activation of the immune system.

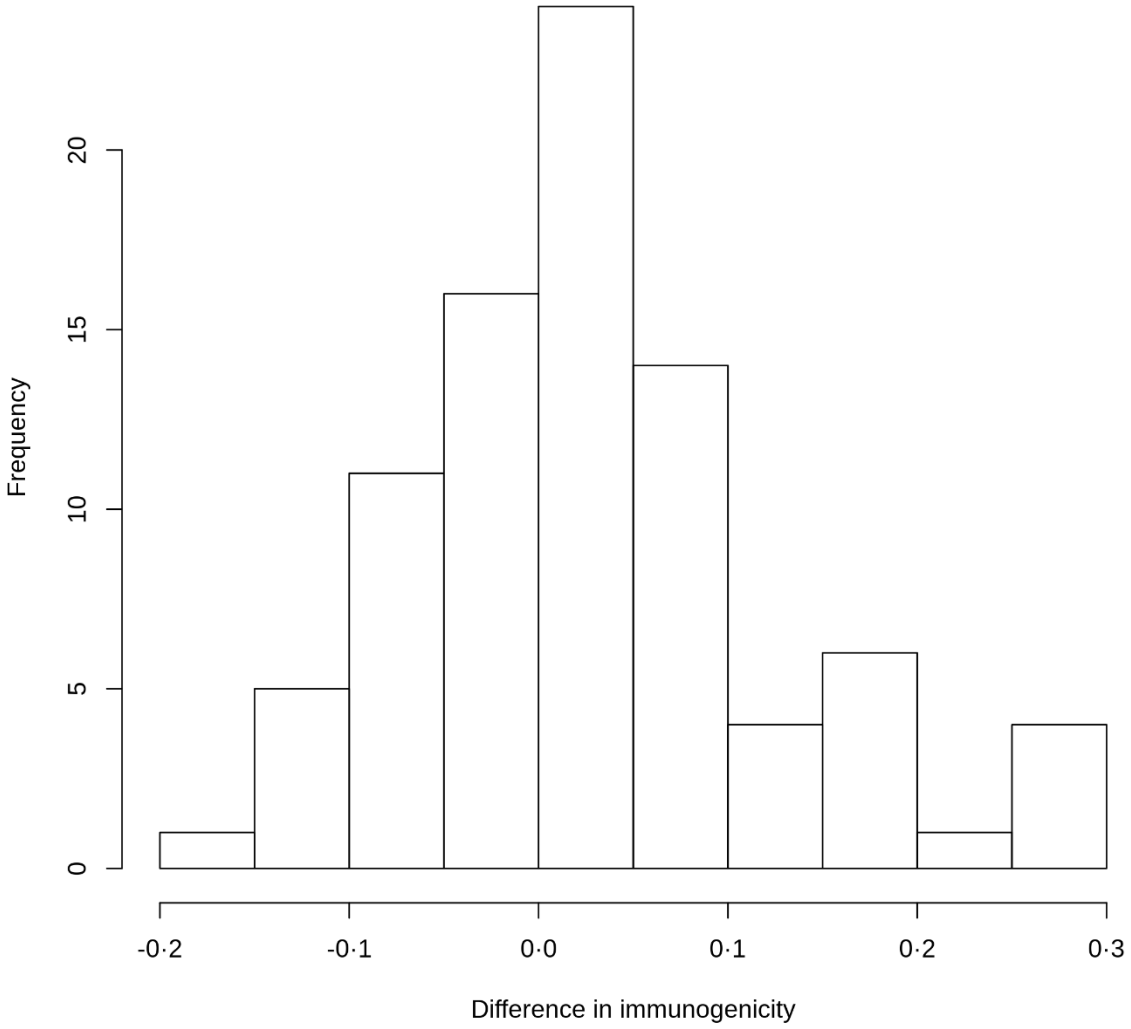

Supplementary Figure 10B: Absolute difference in immunogenicity between wild-type and neoantigen derived epitopes in tumors showing variants associated with proteasomal immune escapes and additional PD-L1 overexpression.

In this figure, a histogram representing the absolute differences in the immunogenicity between epitopes derived from mutant sequences compared to those derived from their wild-type counterparts in tumors showing variants associated with proteasomal immune escapes and additional PD-L1 overexpression. Negative values indicate an enhanced, positive values a lowered potential of activating the immune system. A vast majority of mutant epitopes reduce the immunogenic potential of the altered epitopes compared to the wild-type ones. In addition, only very few fragments show a biologically significant increase in their TCR activation potency. Overall, no activation of T-cell driven anti-cancer immunoreaction can be approximated even when reactivating hosts immune system.

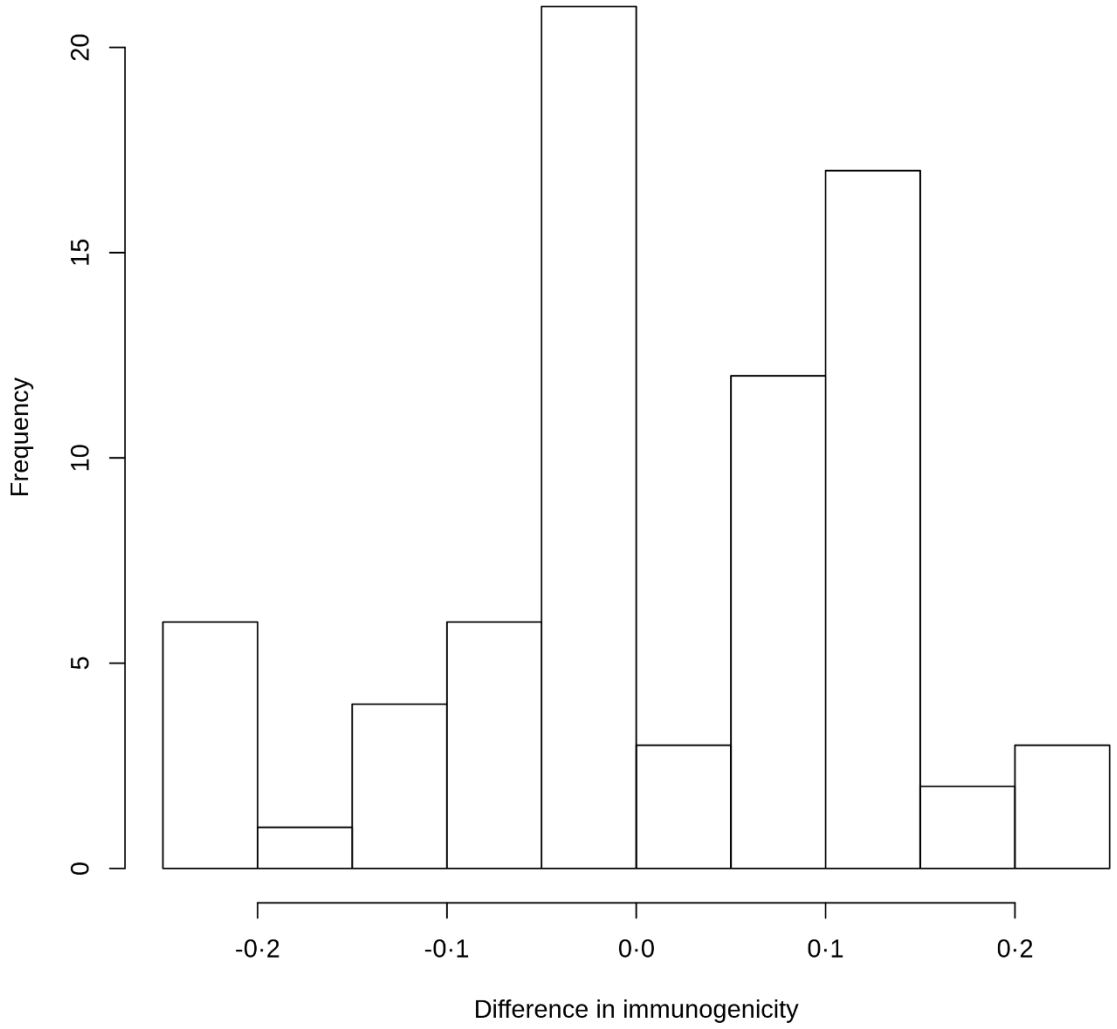

Supplementary Figure 10C: Absolute difference in immunogenicity between wild-type and neoantigen derived epitopes in tumors showing variants associated with proteasomal immune escapes without PD-L1 overexpression.
The histogram illustrates the absolute differences in the immunogenicity between epitopes derived from mutant sequences compared to those derived from their wild-type counterparts in in samples showing variants associated with proteasomal immune escapes without PD-L1 overexpression. Negative values indicate an enhanced, positive values a lowered potential of activating the immune system. A major number of mutant epitopes reduce the immunogenic potential of the altered epitopes compared to the wild-type ones; the majority of the remaining fragments does not affect their immunogenicity. However, there is a portion showing a biologically significant increase in their TCR activation potency, reflecting a reduced but not removed potential to induce hosts immune system.

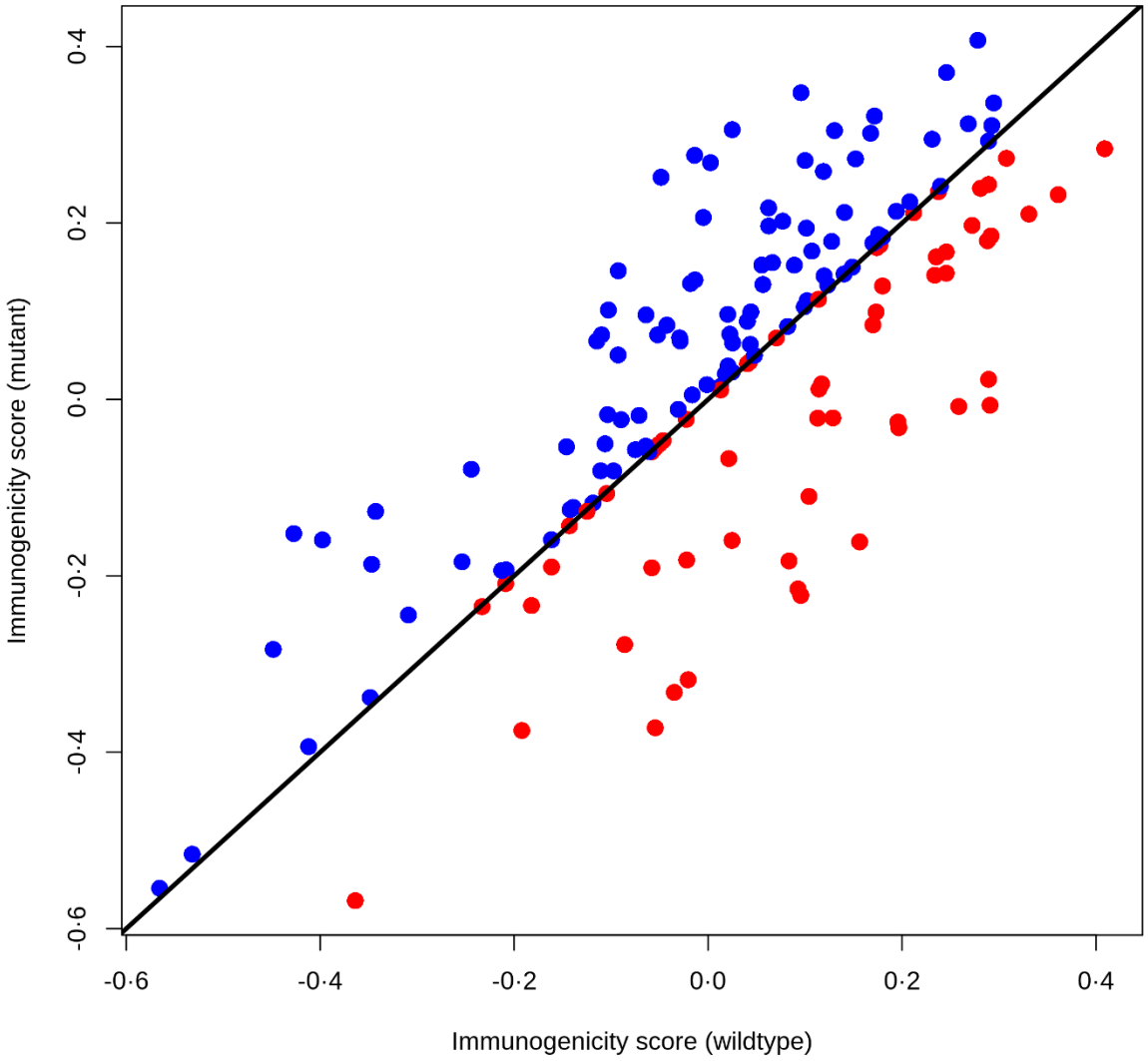

Supplementary Figure 11A: Comparison of immunogenicity between mutant and wild-type derived epitopes in cases showing no variants associated with proteasomal immune escapes.

Suppl. figure 11A depicts a dot plot indicating differences in immunogenicity between epitopes derived from samples without evidence for proteasomal processing escapes. X-axis shows negative immunogenicity scores for wild-type derived; y-axis shows negative immunogenicity scores for variant-derived epitope fragments. Red dots indicate a higher likelihood of immunoactivation of wild-type derived fragments, blue dots a higher likelihood for variant-derived epitope fragments. Overall, a likely equal distribution around the abline could be observed, with a slight overhead in immune activation of altered fragments.

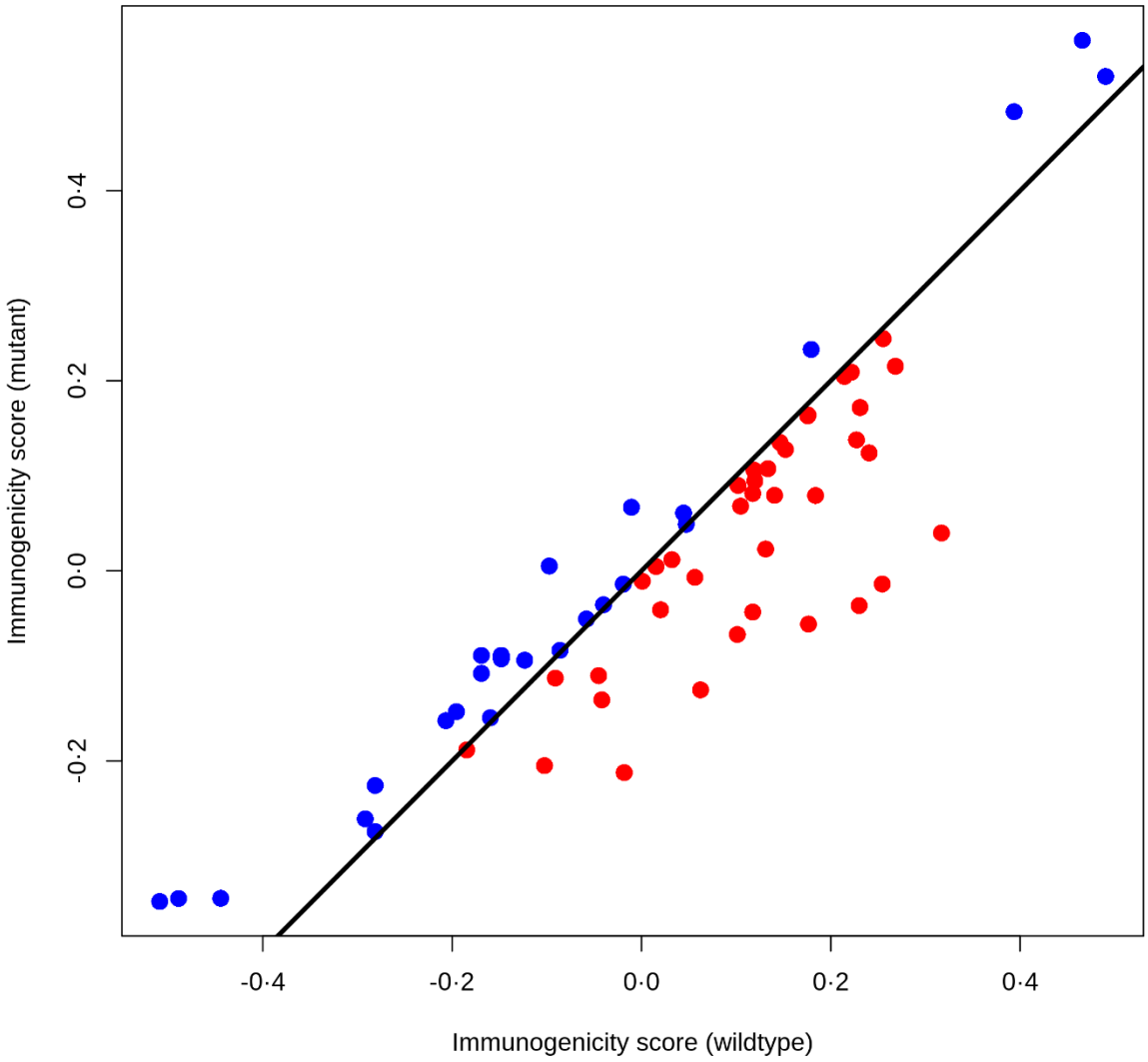

Supplementary Figure 11B: Comparison of immunogenicity between mutant and wild-type derived epitopes in cases showing variants associated with proteasomal immune escapes and additional PD-L1 expression.

Suppl. figure 11B depicts a dot plot indicating differences in immunogenicity between epitopes derived from samples showing variants associated with proteasomal immune escapes and additional PD-L1 expression. X-axis shows negative immunogenicity scores for wild-type derived; y-axis shows negative immunogenicity scores for variant-derived epitope fragments. Red dots indicate a higher likelihood of immunoactivation of wild-type derived fragments, blue dots a higher likelihood for variant-derived epitope fragments. Those processing escape associated epitopes show a clearly reduced potential of activating the hosts immune system, reflected by the large proportion of red dots.

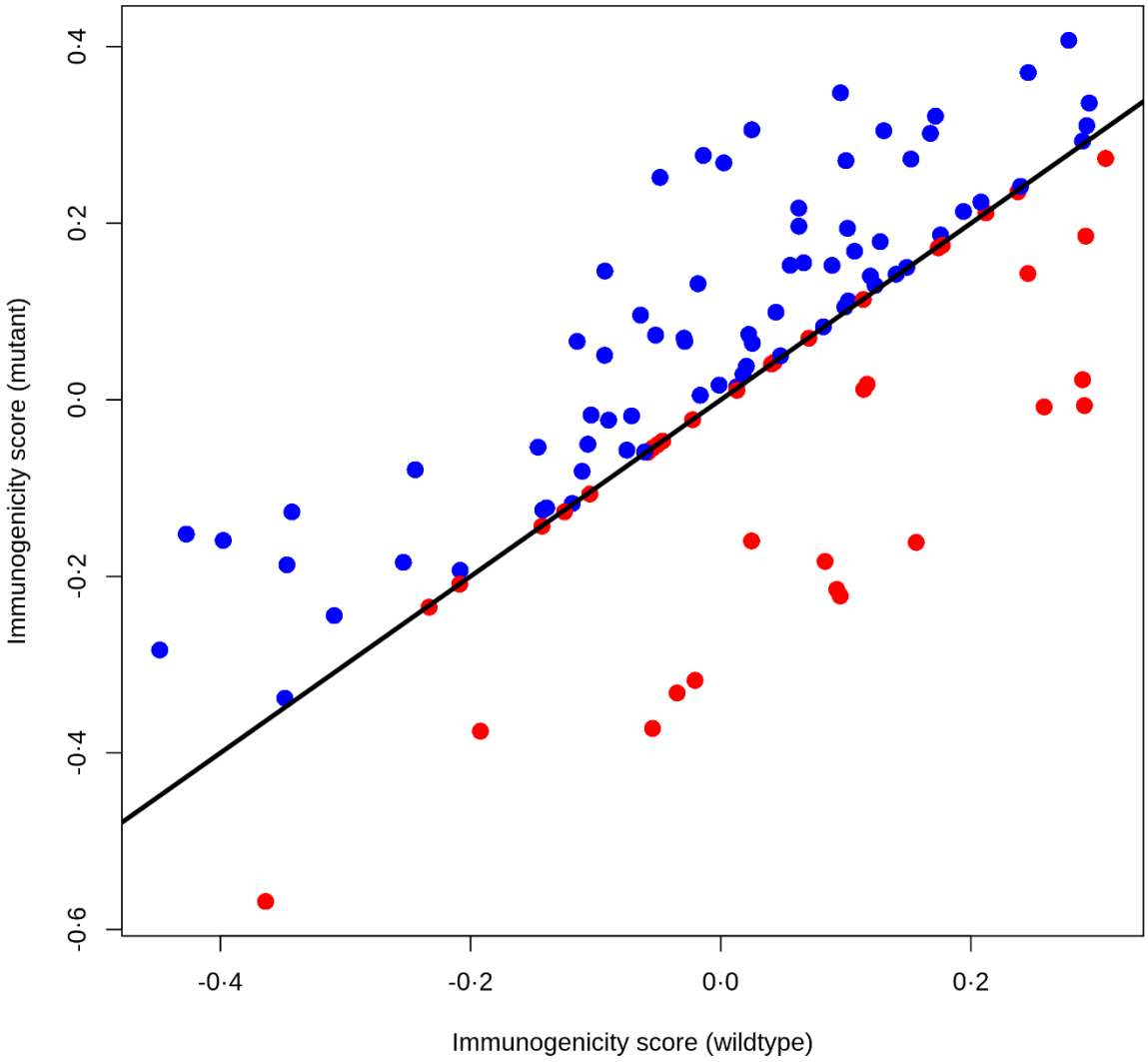

Supplementary Figure 11C: Comparison of immunogenicity between mutant and wild-type derived epitopes in cases showing variants associated with proteasomal immune escapes without PD-L1 expression.

Suppl. figure 11A depicts a dot plot indicating differences in immunogenicity between epitopes derived from samples showing variants associated with proteasomal immune escapes without PD-L1 expression. X-axis shows negative immunogenicity scores for wild-type derived; y-axis shows negative immunogenicity scores for variant-derived epitope fragments. Red dots indicate a higher likelihood of immunoactivation of wild-type derived fragments, blue dots a higher likelihood for variant-derived epitope fragments. Overall, a likely equal distribution between wild-type and variant-derived epitopes can be observed, with a tendency of overrepresentation in immune activation of altered fragments.

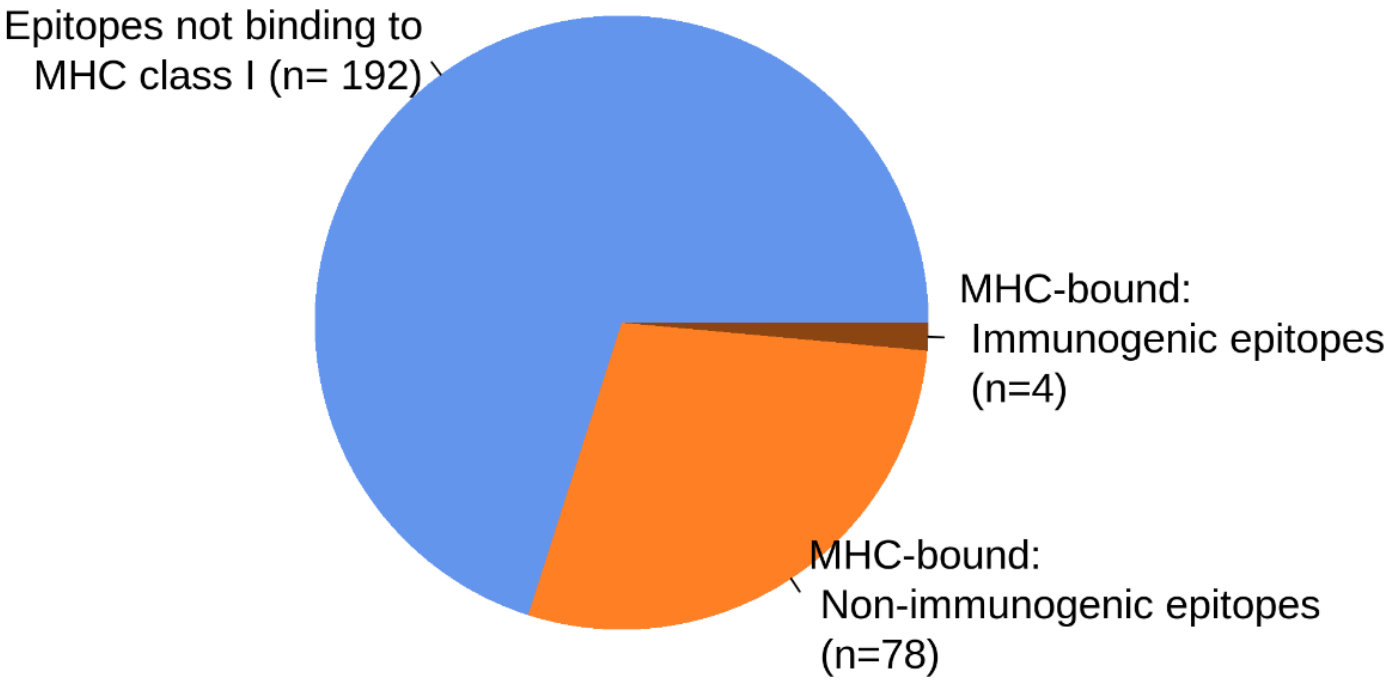

Supplementary Figure 12: Pie chart overview of combining presentation fo altered epitope fragments and their immunogenicity

The figure illustrates the distribution of MHC-I binding affinity and immunogenicity of processing-escape associated predicted epitope fragments. Of those 274 estimated epitopes, 192 show no affinity to bind MHC-I molecules. Of the remaining 82 epitopes, the vast majority (78) show no evidence for a potential to induce an active anti-cancer immune response. Only the remaining 4 still seem to be presented and potent to trigger an immune response, excluding them from processing escape associated variants.

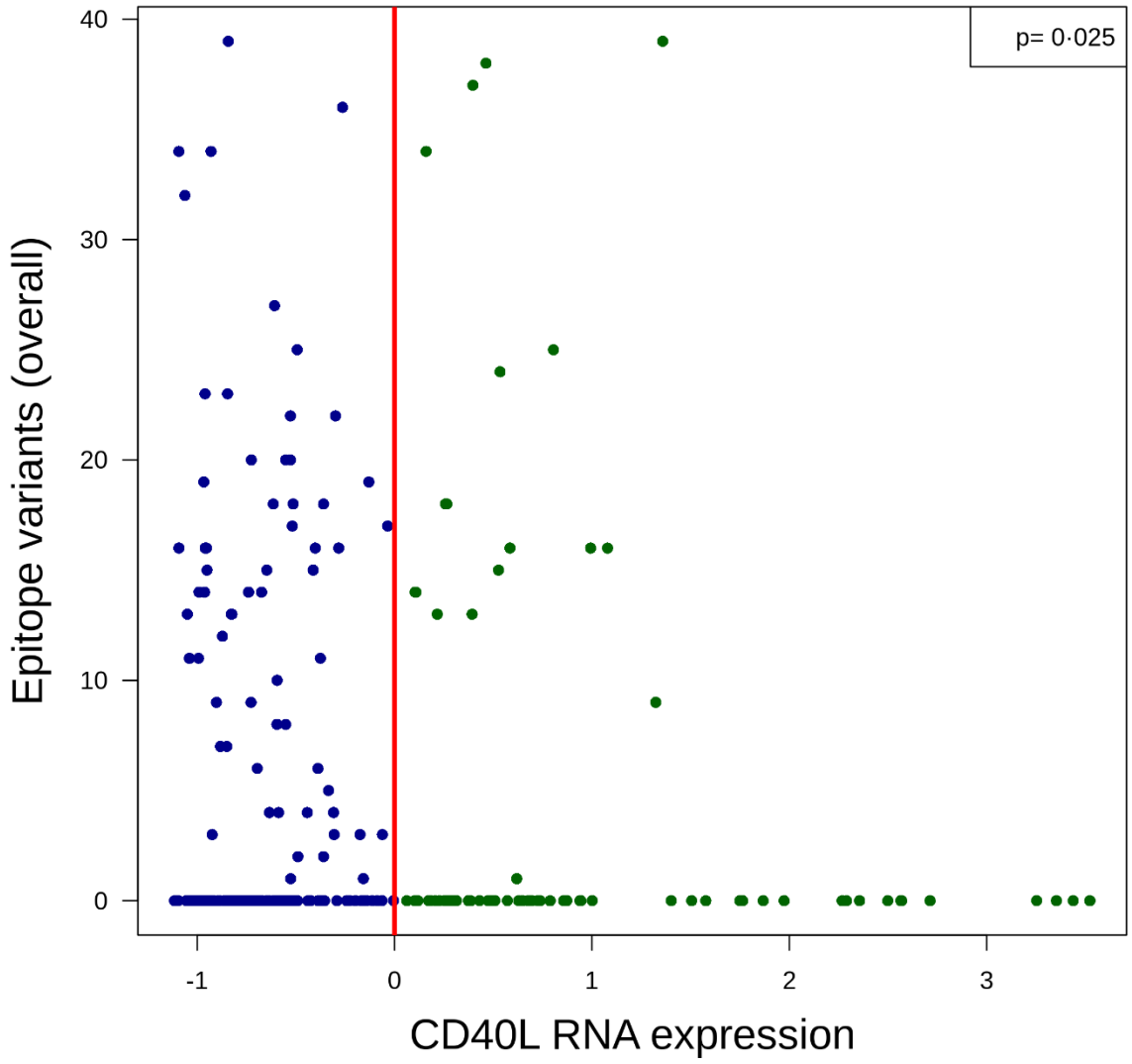

Supplementary Figure 13A: Influence of the number of altered epitope fragments affected by proteasomal processing escapes per sample and immune infiltration depicted by CD40L.

The dot plot illustrated the association between the number of altered epitope fragments affected by proteasomal processing escapes per sample and the detected CD40L mRNA expression of the same area by whole-transcriptome sequencing. A significant association between reduced immune infiltration of CD40L positive cells and a high number of processing-escape associated epitope fragments can be observed. Of note, the figure strongly indicates processing escapes as one, but not the only mechanism of tumors immune escape, as a gross of samples with reduced immune activity still shows no appearance of processing escape associated mutations, indicating alternative mechanisms. Additionally, few samples with high epitope counts and no reduced immune infiltration can be found, that may reflect the PD-L1 negative group.

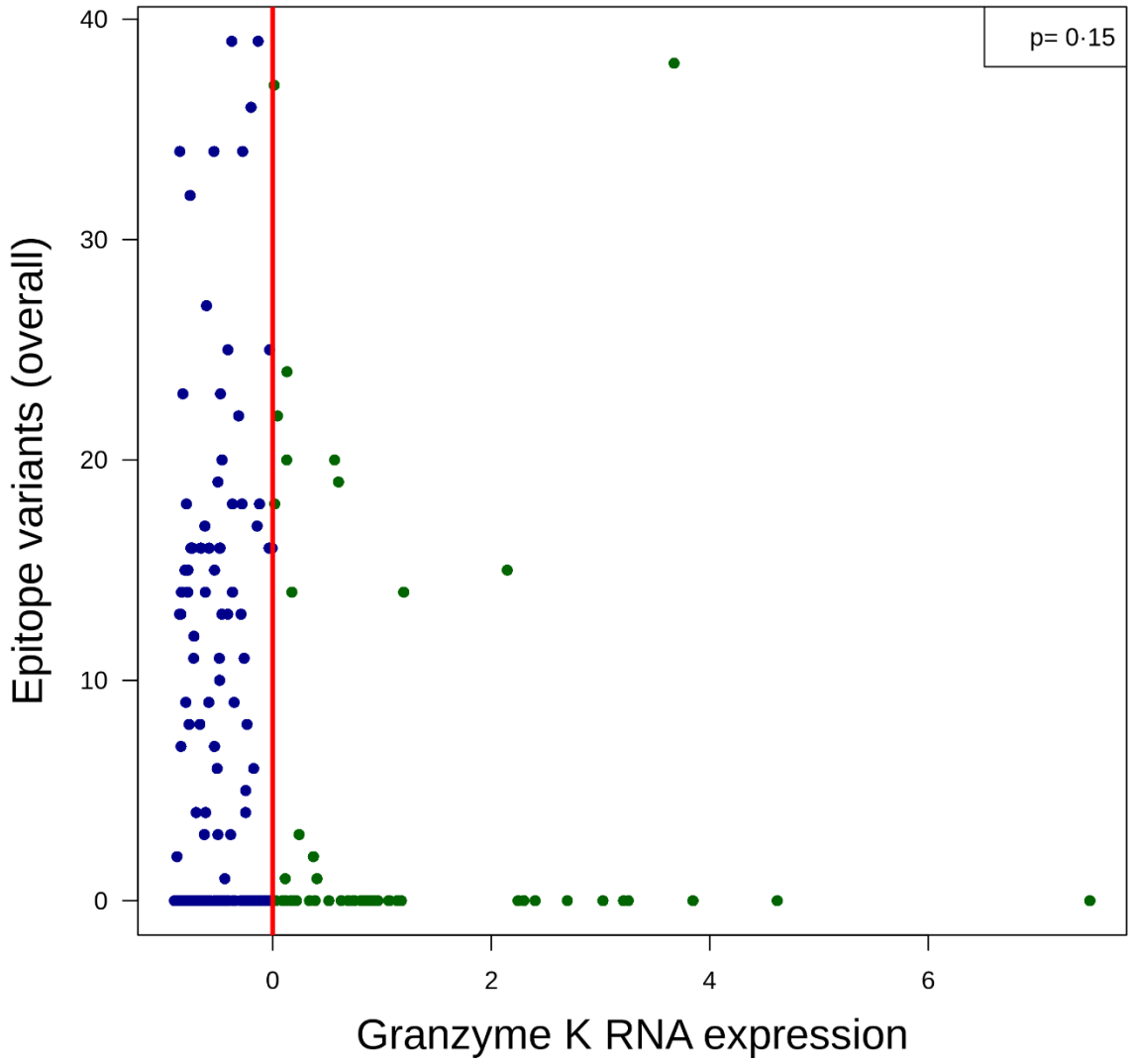

Supplementary Figure 13B: Influence of the number of altered epitope fragments affected by proteasomal processing escapes per sample and active anti-cancer immune response depicted by GZMK mRNA expression.

The dot plot illustrated the association between the number of altered epitope fragments affected by proteasomal processing escapes per sample and the detected GZMK mRNA expression of the same area by whole-transcriptome sequencing. A significant association between reduced number of active killer cells depicted by mRNA expression levels of different granzymes (GZMK exemplarily shown) and a high number of processing-escape associated epitope fragments can be observed. Of note, the figure strongly indicates processing escapes as one, but not the only mechanism of tumors immune escape, as a gross of samples with reduced immune activity still shows no appearance of processing escape associated mutations, indicating alternative mechanisms. Nevertheless, it is strikingly that nearly all samples showing processing escapes have no or strongly reduced granzyme expression at all.

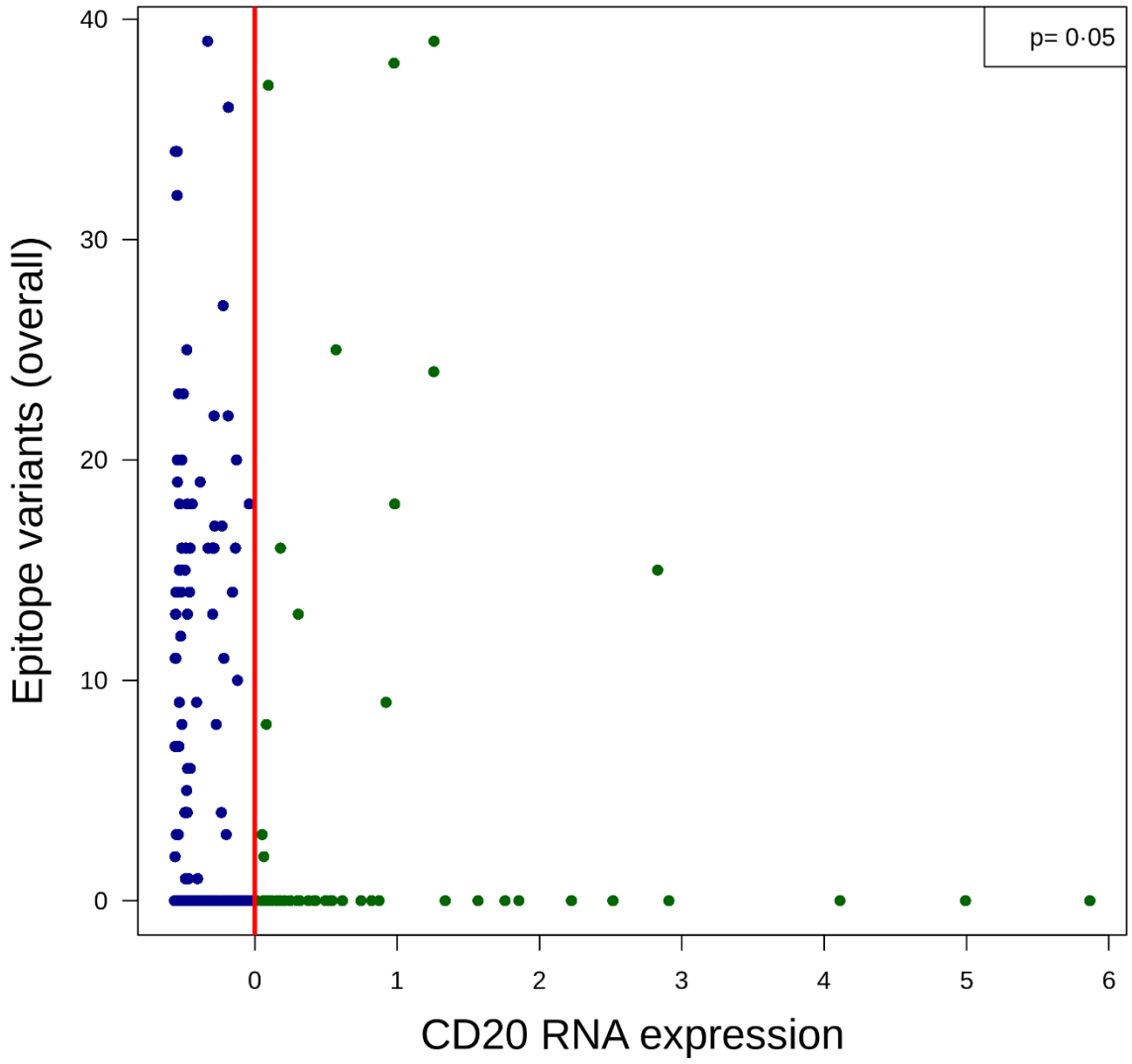

Supplementary Figure 13C Influence of the number of altered epitope fragments affected by proteasomal processing escapes per sample and immune cell infiltration beside T-cells and T-cell response associated immune cells depicted by CD20 mRNA expression.

The dot plot illustrated the association between the number of altered epitope fragments affected by proteasomal processing escapes per sample and the detected CD20 mRNA expression of the same area by whole-transcriptome sequencing. A significant association between reduced immune infiltration of CD20 positive B-cells and a high number of processing-escape associated epitope fragments can be observed. Of note, the figure strongly indicates processing escapes as one, but not the only mechanism of tumors immune escape, as a gross of samples with reduced immune activity still shows no appearance of processing escape associated mutations, indicating alternative mechanisms. Additionally, few samples with high epitope counts and no reduced immune infiltration can be found, that may reflect the PD-L1 negative group. Recent research indicates an underestimated influence of B-cell in host's anti-cancer immune response.